NASA CONTRACTOR REPORT

NASA CR-1386

THE INTERACTION AND PENETRATION OF GASEOUS JETS IN SUPERSONIC FLOW

by R. C. Orth, J. A. Schetz, and F. S. Billig

Prepared by
JOHNS HOPKINS UNIVERSITY
Silver Spring, Md.
for

NATIONAL AERONAUTICS AND SPACE ADMINISTRATION • WASHINGTON, D. C. • JULY 1969

NASA CR-1386

THE INTERACTION AND PENETRATION OF GASEOUS JETS IN SUPERSONIC FLOW

By R. C. Orth, J. A. Schetz, and F. S. Billig

Funded by NASA, Contract No. R-76 and prepared under Naval Ordnance Systems Command Contract No. NOw-62-0604-c by Johns Hopkins University, Applied Physics Laboratory, Silver Spring, Md.

for

NATIONAL AERONAUTICS AND SPACE ADMINISTRATION

For sale by the Clearinghouse for Federal Scientific and Technical Information
Springfield, Virginia 22151 – CFSTI price $3.00

THE INTERACTION AND PENETRATION OF GASEOUS JETS IN SUPERSONIC FLOW

by

R. C. Orth, J. A. Schetz, and F. S. Billig

Johns Hopkins University
Applied Physics Laboratory
Silver Spring, Maryland

SUMMARY

Experiments and analysis of the penetration of a gaseous jet from a discrete orifice into a supersonic stream and the associated interaction with the external flow are discussed. Included in the interaction is the definition of the shape of the stand-off shock in the main flow. A governing parameter in this analysis is the degree of underexpansion of the jet which has been shown to be directly related to the ratio of jet static pressure to the pressure downstream of a strong disturbance in the main stream. For underexpanded jets the location of the Mach disk which is paramount to the definition of the penetration has been explicitly given. For matched pressure injection or for the region of flow downstream of the Mach disk, a solid body drag model has been revised and extended to describe the penetration into a supersonic stream.

The study encompassed the effects of free stream Mach number, hole size and shape and the molecular weight, Mach number, and pressure of the injectant. An exemplary case of the design of the injectors for a typical supersonic combustor is given.

NOMENCLATURE

a	=	speed of sound
$A(s)$	=	jet cross-section area
b	=	separation height
C_D	=	drag coefficient, D/hds
D	=	drag, or combustion chamber diameter
d_j	=	initial jet diameter
d_j^*	=	equivalent jet diameter at sonic conditions
ER	=	fuel/air equivalence ratio
g	=	acceleration of gravity = 32.17 ft/sec^2
h	=	width of jet
m	=	mass
$\dot{m}$	=	mass flow rate
M	=	Mach number
n	=	number of injection ports
P	=	static pressure
$\overline{P}$	=	average pressure over jet cross section
P_b	=	effective back pressure = $\frac{2}{3} P'_{ta}$
q	=	$\rho u^2/2$ = dynamic pressure
r_j	=	radius of jet
R	=	radius of curvature
R_B	=	equivalent body nose radius
s, $\overline{s}$	=	distance along jet axis; $\overline{s} \equiv s/d$
t	=	time
T	=	temperature
u	=	axial velocity in jet

u_a = velocity in undisturbed air stream

u_j = initial jet velocity

x = downstream distance from the injector port

x_0 = abscissa of center of Mach disk

$\tilde{\tilde{x}}$ = arbitrary downstream location, Eq.(19)

y = normal distance from the plate surface

y_0 = ordinate of Mach disk

$\tilde{y}$ = ordinate of outer jet boundary

z = total displacement of Mach disk, Eq.(13)

α, α_0 = angle of jet incidence and initial value

α_1 = limiting angle in Eq. (12)

α_2 = angle of jet incidence at edge of separation layer

β = displaced height of shock inflection point

γ = ratio of specific heats

δ = boundary layer thickness ahead of jet

Δ = shock stand-off distance

η_{ke} = inlet kinetic energy efficiency

ϵ = $(1 + \frac{\gamma-1}{2})/(1 + \frac{\gamma-1}{2} M^2)$

ρ = density

Subscripts

a = undisturbed mainstream conditions

j = initial jet conditions

js = initial conditions for supersonic injection

t = total conditions

∞ = free stream conditions

Superscripts

$( )'$ = conditions following normal shock in main stream

$( )^*$ = conditions corresponding to sonic point in jet

ILLUSTRATIONS

Figure

1 Schematic Representation of Jet Centerline Trajectory.

2 Values of the Integral in Equation (11) for Various Free Stream Mach Numbers.

3 Secondary Jet Structure.

4 Penetration for Two Free Stream Conditions with the Same Ratio, $\rho_j v_j^2/\rho_a u_a^2$.

5 Penetration for a Typical Case with Injection at Two Angles to the Free Stream.

6 Flat Plate Injector and Mach 2.72 Free Jet Nozzle.

7 Ratio of Total Injectant Pressure to Free Stream Effective Back Pressure Versus Mach Disc Distance.

8 Jet Trajectory and Injectant Concentration Profiles for Matched-Pressure Sonic Injection.

9 Jet Trajectory and Injectant Concentration Profiles for Under-Expanded Sonic Injection.

10 Jet Trajectory and Injectant Concentration Profiles for Supersonic Injection.

11 Flat Plate Injector with Three Directional Moveable Probe.

12 Schlieren Photographs of Fine Jet Structure of Underexpanded Sonic Jets (p_j/p_b = 5.23) in a Mach 2.1 Stream.

13 Effect of Injector Shape on Jet Structure for Underexpanded Sonic Injection into a Mach 2.1 Supersonic Stream.

14 Concentration Profiles for Underexpanded Sonic Injection into a Mach 2.7 Stream.

15 Ratio of Perpendicular to Longitudinal Mach Disc Distance Versus Ratio of Total Injectant Pressure to Effective Back Pressure.

16 Maximum Concentration Locus for Sonic H_2 Injection into Mach 2.72 Air Stream, Comparison of Data with Various Equations.

Figure

17 Jet Boundary for H_2 Injection into Mach 2.72 Air Stream Comparison of Data with Eq. (18).

18 Measured Penetration (y_s/y) at Various Downstream Locations for 10^o Conical Supersonic Injectors.

19 Shock Wave Displacement Correlation.

20 Shock Shape for Sonic Air Injection.

21 Shock Shape for Sonic Hydrogen Injection.

22 Shock Shape for Various Shapes of Injection Port.

23 Combustion Chambers for Mach 6 Flight of a Scramjet with Stoichiometric Hydrogen Injected.

INTRODUCTION

In recent years there has been considerable interest in the flowfield produced by the angular injection of fluid (liquid or gas) through discrete openings in a wall into an otherwise uniform supersonic stream. Past work in this area has been aimed primarily at aerodynamic control systems;[1-8] consequently, major emphasis has been placed on the pressure field produced on the surface near the injection station. The development of scramjet engines, which require fuel injection into a supersonic airflow, has underscored the importance of understanding the mechanism of jet penetration so that the resulting jet trajectory and fuel-air mixing can be predicted.

The main contribution of prior work on penetration is the presentation of reliable experimental data and correlations of various injector and free-stream parameters. Most often used are the injectant-to-free-stream pressure and momentum ratios.[7-11] These correlations are based on data measured at stations more than ten injector diameters downstream from the injector ($x/d_j > 10$). Thus, they provide estimates of the gross performance of the injectors, but the results are insufficient for a clear understanding of the jet penetration in the near downstream region ($x/d_j < 10$).

The analytical work has generally been rather crude, involving one or more of the following untenable assumptions: 1) the injected flow turns sharply and then follows the surface; 2) the shape of the turning jet is semicylindrical; 3) the flow in the jet is homentropic; 4) mixing is instantaneous at the injection station and dissipates the transverse jet momentum; 5) small disturbance theory can predict the pressure field; 6) the jet acts as a rigid vertical obstruction with some arbitrary height; 7) the total injectant penetrant is the height of the first Mach disk in an underexpanded jet; and 8) the transverse momentum of the jet remains constant.

This report describes the analytical and experimental work done at APL in the area of jet penetration over the past three years. Portions of the work have been previously described in abridged forms (Ref. 12-19).

ANALYSIS

JET TRAJECTORY ANALYSIS

The interaction of a secondary jet and subsequent dispersion into the primary fluid is assumed to be a two-stage process. In the penetration stage, the jet retains its identity while being accelerated and turned in the flow direction of the primary fluid. The second stage is considered to be a coaxial turbulent mixing process and is not discussed herein. We shall retain the assumption that has been used in subsonic analyses[8] that the jet acts as some "solid" body that emerges from the port and is bent downstream by drag and distorted in cross-section

by pressure differences on the front and back faces and viscous shear. Two general cases are considered, viz., the "on design" case in which the pressures of the jet and the main stream are nearly matched, and the underexpanded jet. In the latter case, the turning and distortion of the jet is preceded by a rapid area expansion and normal shock. The analysis for this case is identical with the former except that the initial conditions (density, velocity, cross-sectional area, and angle) correspond to the conditions following the normal shock, and the height to the normal shock or Mach disk is superposed to the penetration depth. The horseshoe-shaped cross section of the turning jet which has been observed experimentally[7,8] is approximated as an ellipse, and the growth of the width is taken from subsonic measurements.[8] The drag coefficient on an element of the jet "body" is taken as that for an infinite cylinder at the local angle of incidence to the stream.[20]

Consider the forces acting on an infinitesimal length ds of the jet cross section, as shown in Fig. 1. First, balancing forces along the jet axis,

$$m(du/dt) = -mg \sin \alpha + \Delta\bar{P}A \tag{1}$$

where $\Delta\bar{P}$ is the change in average static pressure acting over the cross section in going from s to s + ds. Then, balancing forces on an element of mass m in a direction perpendicular to the axis,

$$D + mg \cos \alpha = mu^2/R \tag{2}$$

where u = u(s) is the local jet velocity and R = R(s) is the radius of curvature of the jet centerline. Now, an increment of time dt is related to the length and velocity by dt = ds/u, which can be substituted into Eq. (1). Furthermore, ds = Rdα, and $D = C_D q_a (\sin^2\alpha)$ hds, where h is the local width of the jet measured in the plane perpendicular to the plane in the sketch in Fig. 1. Generally, the forces due to drag and inertia are large compared to gravity forces, and the latter can be neglected. With this assumption and the foregoing substitutions, Eqs. (1) and (2) become

$$\rho u(du/ds) = -d\bar{P}/ds \tag{3}$$

$$d\alpha/ds = -C_D h q_a \sin^2\alpha/\rho u^2 A \tag{4}$$

Since ρuA is the mass flow in the jet, which remains constant at the initial value, Eq. (4) can be put in the form

$$\frac{d\alpha}{ds} = -\frac{C_D h \rho_a u_a^2 \sin^2\alpha}{2\rho_j u_j^2 (A_j^2/A)(\rho_j/\rho)} \tag{5}$$

When u is eliminated from Eq. (4) in this way, it is not necessary to consider Eq. (3) to obtain the solution if h(s), A(s), ρ(s), and $C_D(\alpha)$ are known. The last item can be determined by assuming that

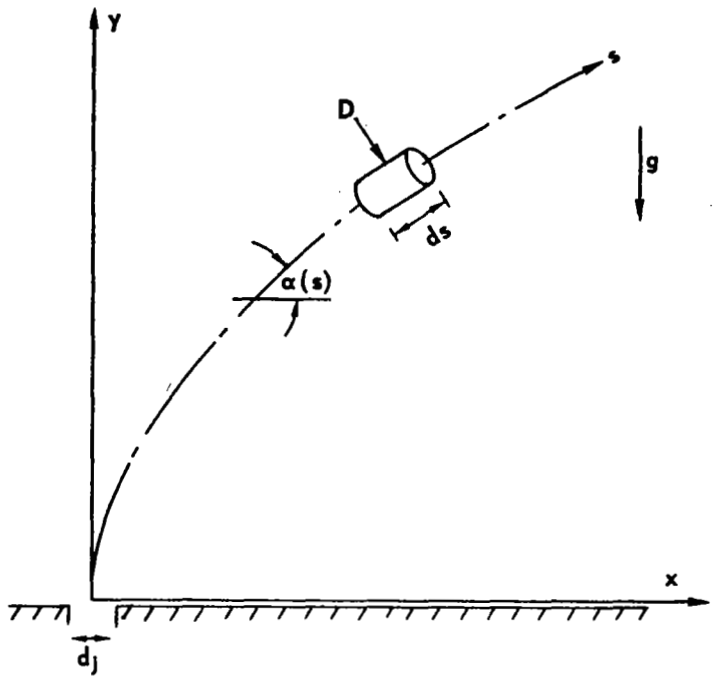

Fig. 1 SCHEMATIC REPRESENTATION OF JET CENTERLINE TRAJECTORY

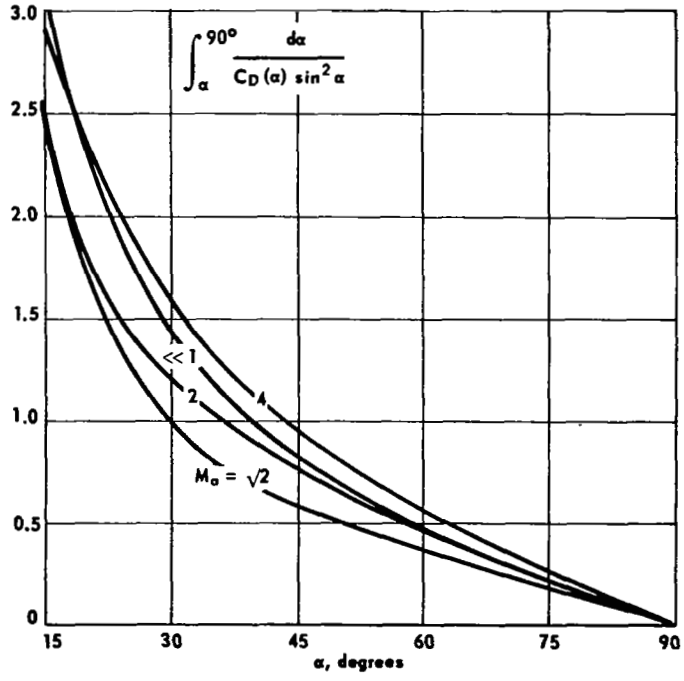

Fig. 2 VALUES OF THE INTEGRAL IN EQUATION (11) FOR VARIOUS FREE STREAM MACH NUMBERS

each element of the jet acts as an element of an infinite cylinder aligned at the local angle to the flow. Experimental data are available for this situation,[20] and the following simplified curve fits are taken as an adequate representation of these data:

$$C_D = 1.2 + (M_a \sin \alpha)^{7/2} \qquad 0 \leq M_a \sin \alpha \leq 1 \tag{6a}$$

$$C_D = 1.06 + 1.14\,(M_a \sin \alpha)^{-3} \qquad M_a \sin \alpha \geq 1 \tag{6b}$$

From subsonic experiments,[8]

$$h = 2.25\, d_j + 0.22\, s \tag{7}$$

Reference 8 also suggests that the shape of the cross section be taken as an ellipse with a ratio of major to minor axes of 5 to 1. With this and Eq. (7), the A(s) can be determined from

$$A(s) = \pi h^2/20 \tag{8}$$

Furthermore,

$$h(A/A_j^2) = [2.25 + 0.22\,(s/d_j)]^3/2.5\pi d_j \tag{9}$$

Finally, combining Eqs. (9) and (5),

$$\frac{d\alpha}{d\bar{s}} = -\frac{C_D(\alpha)\sin^2(\alpha)}{2.5\pi}\ \frac{\rho_a u_a^2}{\rho_j u_j^2}\ \frac{\rho}{\rho_j}\ (2.25 + 0.22\,\bar{s})^3 \tag{10}$$

where $\bar{s} \equiv s/d_j$, and $C_D(\alpha)$ is obtained from Eq. (6a) or (6b) for the appropriate range of $M_a \sin \alpha$. The only remaining unspecified quantity is $\rho(s)$, which in this analysis is assumed to be equal to the initial value either at the jet orifice or just downstream of the jet shock for underexpanded injection (see next section). Using this assumption, Eq. (10) can be integrated to give

$$\frac{0.88\,(2.5\pi)}{(\rho_a u_a^2/\rho_j u_j^2)} \int_{\alpha}^{\alpha_0} \frac{d\alpha'}{C_D(\alpha')\sin^2(\alpha')} = (0.22\,\bar{s} + 2.25)^4 - 2.25^4 \tag{11}$$

The integral in Eq. (11) is evaluated by choosing a lower limit for the angle of incidence of interest, say 10°. One then integrates from this lower limit to

$$\alpha_1 = \sin^{-1} M_a^{-1} \tag{12}$$

using Eq. (6a) and then from α to α_0 using Eq. (6b). Typical results are given in Fig. 2 for various values of M_a. For $M_a \leq 0.2$, it is sufficient to take $C_D = 1.2$.

Model of the Flowfield for Angular Gaseous Jet Injection

In Fig. 3 are shown schematic representations of typical flowfields that have been observed for angular injection of gaseous jets into a supersonic free stream. There are four separate cases, and the occurrence of each depends upon the size of boundary layer and separation zone ahead of the injector and whether the injection pressure is matched or underexpanded. In general, a shock in the mainstream is caused by the obstruction of the primary flow by the emerging jet. If the pressure rise on the surface caused by this shock would be greater than about three to one, the boundary layer will separate,[31] and an oblique shock off the separated region will intersect the stronger mainstream shock. When the separation zone is small (Fig. 3a and 3b), the jet is immediately exposed to the momentum of the freestream and is displaced. The amount of displacement is, of course, dependent on flow conditions (e.g., $\rho_j u_j^2/\rho_a u_a^2$ and M_a). In any event, the pressure field on the periphery of the emerging jet is extremely complicated. Since the relation of P_j to this pressure field controls the internal structure of the jet flow, as well as the size of the separation zone ahead of the jet zone, some estimate of the pressure field must be obtained.

Even if the pressure field around the jet were known in detail, there is no simple method known for predicting its effect upon the internal flow in the jet. Some insight into this general flow situation can be obtained by studying the much simpler case of a jet entering a quiescent environment.[10,11] The governing parameter for the jet structure in that case is the ratio of P_j to the "back pressure," i.e., P_b for the quiescent medium. With this ratio and γ, the results of Refs. 10 and 11 can be used to determine y_0 and M_j, respectively (Figs. 3b and 3d). To apply these results to the case of a jet exhausting into a moving medium, we introduce here the concept of an "effective back pressure" P_b. If the emerging jet is viewed as a roughly cylindrical obstacle, the static pressure distribution around the periphery would be expected to vary from a maximum at the forward stagnation point down to a low value in the "base" region behind the jet; P_b is expected to be somewhere between these extremes. As a corollary to this argument, there will be a value of P_b such that the structure in the jet is a minimum. The situation is defined as a "matched" pressure case; cases with $P_j > P_b$ are "underexpanded".

Studies at the University of Maryland[21,22] indicated that the average pressure field around a cylindrical protuberance on a flat plate in a supersonic stream was approximately equal to two thirds of the pitot pressure in the stream $\frac{2}{3}P_{ta}'$.[21,22] This criterion is used in the present work to specify matched-pressure injection as that in which the static pressure of the secondary jet (P_j) equals the effective back pressure $P_b = \frac{2}{3}P_{ta}'$. The studies also showed that for the case of underexpanded injection the distance to the first Mach disk was only weakly dependent on the height of the separation zone.[21] The importance of this fact is that the Mach disk location, and

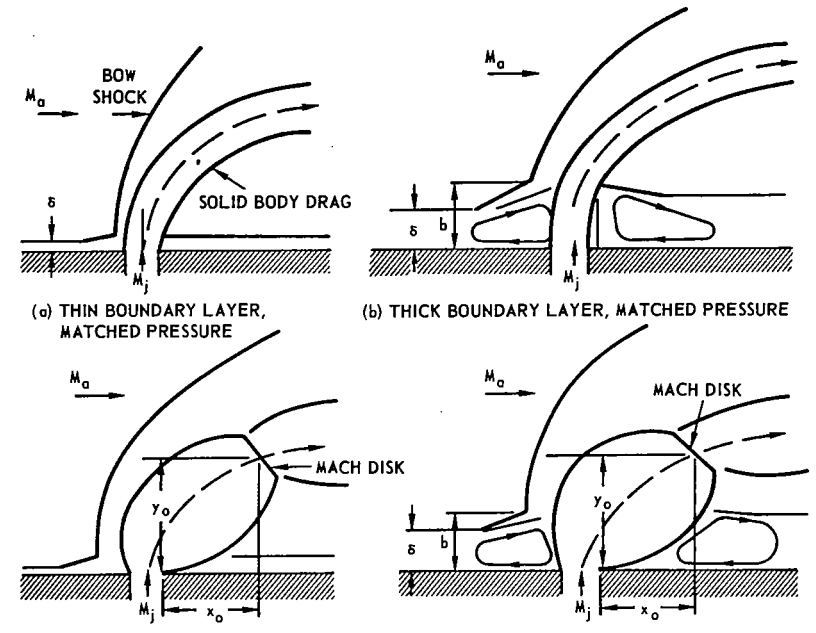

Fig. 3 SECONDARY JET STRUCTURE

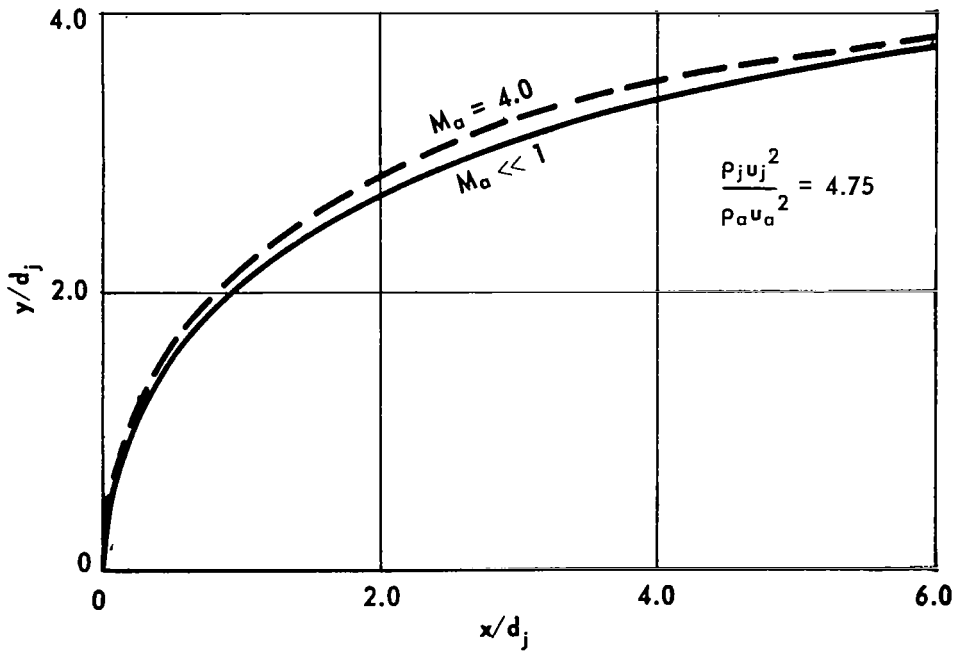

Fig. 4 PENETRATION FOR TWO FREE STREAM CONDITIONS WITH THE SAME RATIO, $\rho_j u_j^2/\rho_a u_a^2$

thus, the value of q_j at that location, can be determined with the knowledge of P_j/P_b. The trajectory calculation is started from that point for all cases of underexpanded injection.

Since the pressure rise associated with matched-pressure injection is sufficient to separate the boundary layer in supersonic flow trajectory, calculations for this case will have to include an estimate of the drag in the separated zone and the separation height b. With these estimates and the assumption that $b/d_j = \bar{s} \sin [(\alpha_j + \alpha_2)/2]$, Eq. (11) can be solved for α_2, the angle of jet incidence at the edge of the separation layer. The trajectory in the freestream can then be calculated using the jet initial conditions and α_2 as the initial angle.

Effects of Initial Conditions on Jet Trajectory

We are now in a position to explore the effects of some simple variations of initial conditions on the fuel jet trajectory. First, consider holding $\rho_j u_j^2/\rho_a u_a^2$ constant while varying M_a. The results of such a comparison are shown in Fig. 4 for $M_a = 4.0$ and $M_a \ll 1$. The interesting, if not surprising, result is that slightly better penetration is achieved for $M_a = 4$. This behavior can be traced to Fig. 2, which shows a lower value of the integral in Eq. (11) for the range $90 < \alpha \leq 18°$. This results in a steeper slope of the curve in this range. The cause of all this is that C_D is lower at high normal Mach numbers ($M_a \sin\alpha$) than for transonic or subsonic values, as evidenced by Eq. (6). Finally, we may observe the effect of α_0 on penetration; results for a typical case are given in Fig. 5.

EXPERIMENTAL PROCEDURE AND TEST RESULTS

The objective of the experimental program was to study the effects of certain parameters on the jet-freestream interaction, i.e., the jet structure and penetration in the near downstream region. The variables examined were the injectant-to-freestream pressure and momentum ratios, injectant and freestream Mach numbers, and the shape of a single injection port. To simulate the design restrictions imposed on a fuel injector by a fixed ER requirement, injectant mass flow was held constant during the parametric variations.

Parametric Variation of Injection Pressure and Mach Number

Experiments were conducted on a flat plate mounted in line with a Mach 2.72 free air jet (Fig. 6). Cold H_2 and N_2 were injected normal to the airstream from an axisymmetric sonic or supersonic nozzle located 1.75 in. from the leading edge of the plate. The supersonic injectors ($M_{j_s} = 1.31$, 1.50 and 1.67) had 10-deg. half-angles. Hydrogen concentration profiles were determined by gas-sampling with a seven-point, movable sampling rake. The samples were analyzed on a Beckman GC-2A Gas Chromatograph, and hydrogen concentration was determined by the peak height method.[23] To verify the accuracy of the analysis the sum of the partial pressures of hydrogen and air was compared with the

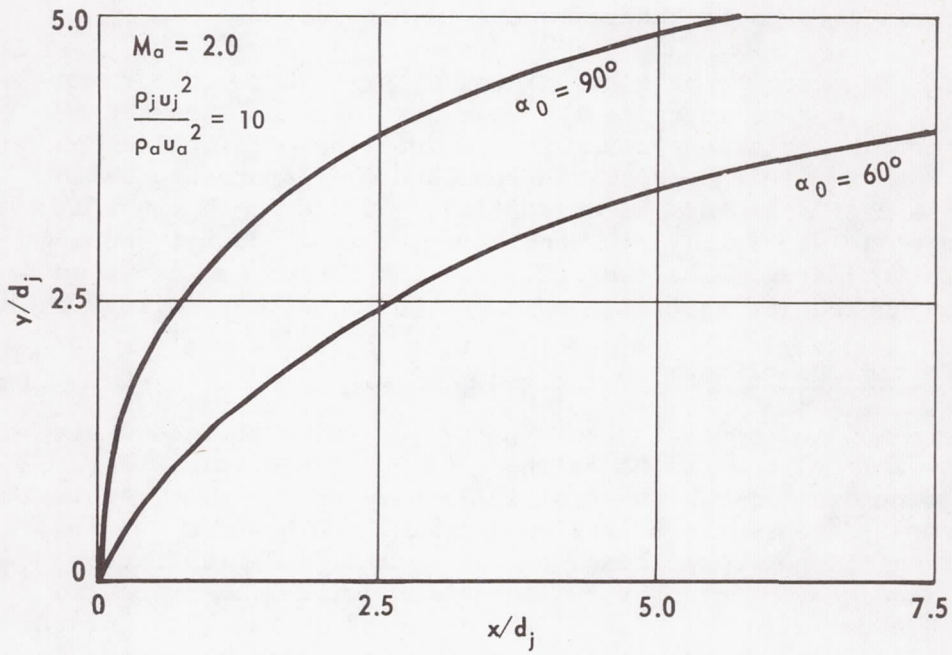

Fig. 5 PENETRATION FOR A TYPICAL CASE WITH INJECTION AT TWO ANGLES TO THE FREE STREAM

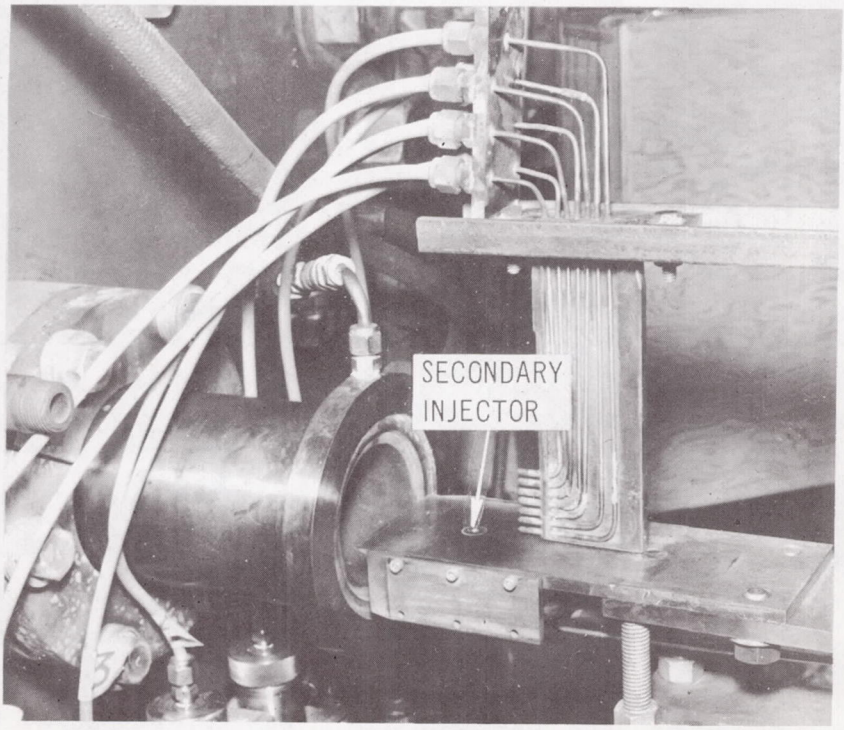

Fig. 6 FLAT PLATE INJECTOR AND MACH 2.72 FREE JET NOZZLE

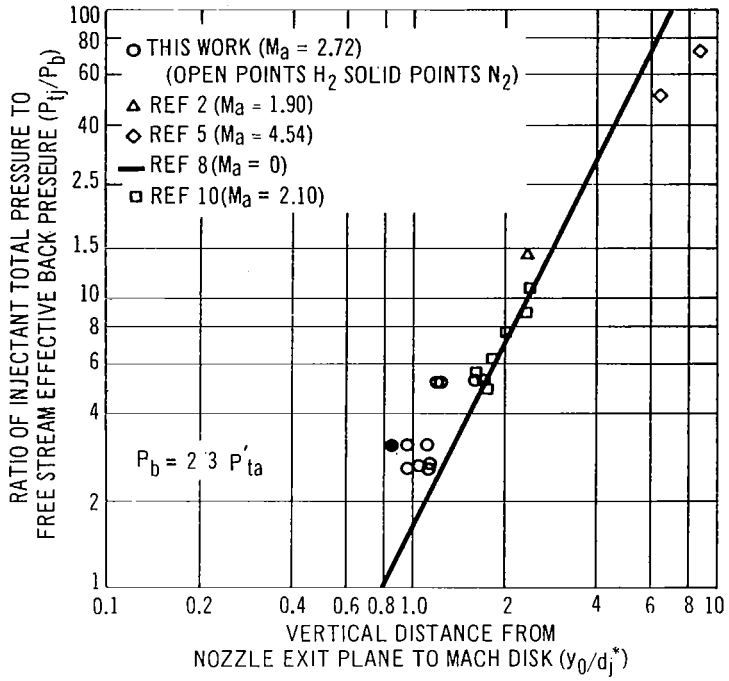

Fig. 7 RATIO OF TOTAL INJECTANT PRESSURE TO FREE STREAM EFFECTIVE BACK PRESSURE VERSUS MACH DISK DISTANCE

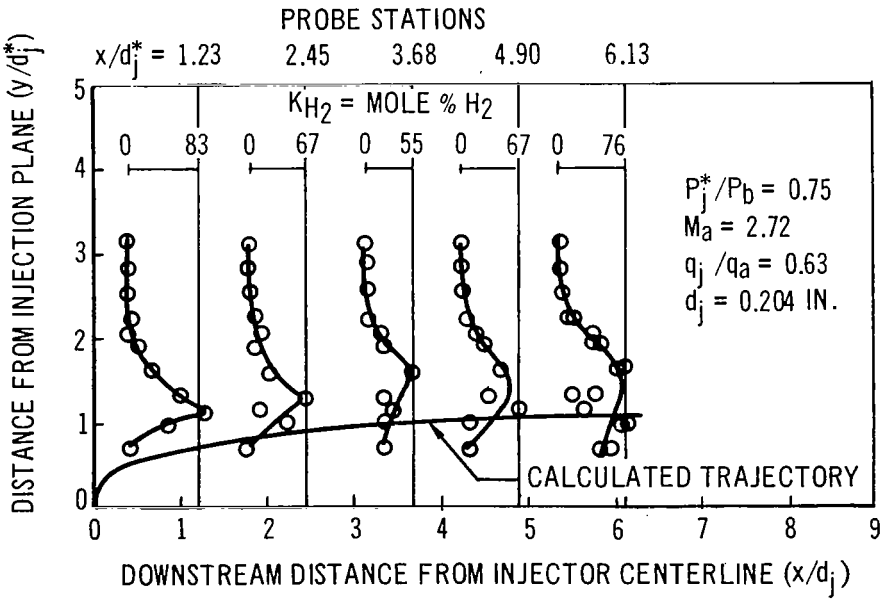

Fig. 8 JET TRAJECTORY AND INJECTANT CONCENTRATION PROFILES FOR MATCHED-PRESSURE SONIC INJECTION

measured total pressure of the sample before analysis. The rms deviation of the summed partial pressures from the measured total pressure was 0.66% and the maximum deviation was 5.3%. This comparison insured that there were no gross errors in the chromatograph analysis. Frequent calibrations using pure known gases were made to detect any contamination of the gas separation column and/or shifting of the sensitivity of the thermal conductivity cell which could cause compensating errors in the measured concentrations of the constitutent gases in an unknown mixture. On the basis of the foregoing procedures we believe that the actual value of hydrogen mole fraction of any one sample was within $\pm$ 2% of the measured value. Pressure measurements were taken periodically in the air and injectant plenum chambers, at the exit wall of the free jet, and in the freestream by using the sampling probe as a pitot probe.

Schlieren photographs were taken on ASA 3000 Polaroid film in a focal-plane camera. They were useful for analysis but, unfortunately, were not of good enough quality to present for publication. For matched-pressure sonic injection ($P_j = P_b$), there was no visual evidence of disturbance within the jet, which simply turned downstream with an outer boundary very close to the limit of the $M \leq 1$ flow region that is shown by the absence of shocks in front of the probes. Strong normal shocks (Mach disks, similar to Fig. 3) were present in both the underexpanded sonic jets and the supersonic jets.

For underexpanded injection, the perpendicular distance from the flat plate to the Mach disk was scaled from the schlieren photographs and plotted vs the ratio of jet total pressure to effective back pressure (P_{tj}/P_b)(Fig. 7). Crist et al. made a thorough investigation of underexpanded jets in a quiescent medium.[10] They showed a relationship between the normalized distance to the first Mach disk (h/d_j) and P_{tj}/P_a. (For a quiescent medium, $P_{ta} = P_a$ or P_∞.) Schetz, Hawkins, and Lehman[21] have extended this concept to injection into supersonic flow by plotting the vertical distance to the Mach disk, y_0/d_j, and the ratio y_0/x_0 vs P_j/P_a'. Note that the correlating effective back pressure P_b used in Ref. 10 is P_a' rather than $\frac{2}{3}P_{ta}'$ and that the quantity $\frac{3}{2}P_a'/P_{ta}'$ varies from 1.18 to 1.33 for $\gamma = 1.4$ and $1.9 < M_a < 4.5$, which is the Mach number range of the data shown in Fig. 7. If the data were normalized on the P_a' basis they would be lowered with respect to the correlating line for the quiescent medium data, thus giving better correlation with some supersonic points but worse with others. Since there was no clear advantage in using P_a' as the correlating parameter, we chose to use $\frac{2}{3}P_{ta}'$ in our presentation to be consistent with the concept of the average pressure around a cylindrical obstruction.

The structure of the emergent supersonic jet was similar to that of the underexpanded sonic jet. The supersonic injectors were designed to give the same static pressure at discharge as the sonic injector for a given mass flow; thus for all supersonic injectors $P_j = P_b$. With coaxial supersonic streams the pressure balance does

occur when the static pressures are matched, and any discrepancies in flow direction from the present conical (rather than contoured) secondary jet are adjusted primarily through a series of weak oblique waves. However, with transverse injection the pressure balance occurs when the static pressures behind strong disturbances in both streams are approximately matched. Whether the secondary jet is conical or contoured is probably relatively insignificant. On this basis the supersonic injectors tested were actually underexpanded, and, therefore, the emergent jets expanded into the main flow until the Mach number was such as to produce the effective back pressure aft of the Mach disk. The values of y_0/d_j^* for the supersonic cases were from 9 to 30% higher than those for underexpanded sonic injection with an equal injectant stagnation pressure. There was also less downstream displacement of the Mach disk than with the equivalent underexpanded sonic jet; however, additional data, particularly at higher values of M_j, is required to produce a correlation of x_0, y_0, and P_{tj}/P_b for supersonic injection.

The injectant concentration profiles (Fig. 8-10) were developed from a best fit to the experimental data of the types of concentration profiles reported by Zukoski and Spaid.[7]

Injector Shape Variations

Two different experimental set-ups were used to study the effect of individual injector shapes on penetration. The first series of tests was conducted in a two-dimensional Mach 2.1 wind tunnel. Helium and air were injected transversely from a flat plate, using three different sonic injector configurations: a circular-ended, 1/4-in. by 1/16-in. slot with its long axis aligned with the main stream flow; the same slot with the long axis perpendicular to the main stream flow; and a 0.136-in.-diameter circular nozzle. The cross-sectional area of the circular nozzle was equal to that of the slot. Injectant-to-freestream pressure ratio, injectant mass flow, and freestream Mach number were held constant, and penetration was determined from schlieren photographs, using air as the injectant, and from gas samples using He as the injectant.

The second series of tests was designed to study the jet trajectory in detail and to provide information on the shape of the jet cross-section in off-axis planes. The experiments were run in a Mach 2.7 free-jet with injection of hydrogen from the flat plate model shown in Fig. 11. The injection port diameter was increased from 0.14 in. to 0.20 in. to aid in the visualization of the flowfield with schlieren. The elongated slot injector was geometrically similar to its previously tested counterpart. The important jet penetration parameters, p_{tj}/p_b and q_j/q_a, were closely matched in the two tests. At Mach 2.1 those ratios were 6.5 and 3.5, and at Mach 2.7 they were 5.92 and 2.8. The sampling station was at $x/d_j = 9.2$ in the former and at $x/d_j = 5$ and 10 in the latter. Gas samples were taken at off-axis locations with a seven-point probe that could be translated in three directions. Improvements in gas chromatography techniques and

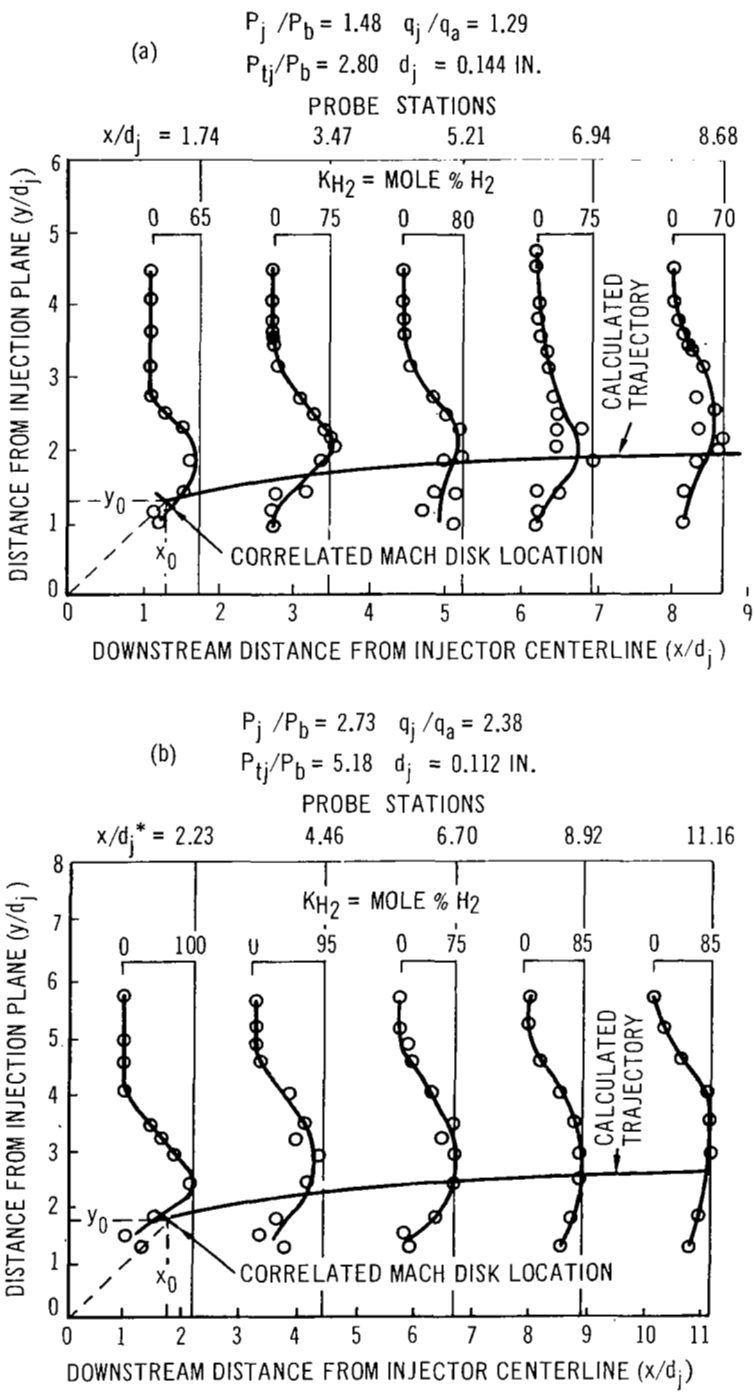

Fig. 9 JET TRAJECTORY AND INJECTANT CONCENTRATION PROFILES FOR UNDER-EXPANDED SONIC INJECTION

(a) $P_j/P_b = 1.00$ $q_j/q_a = 1.50$ $M_j = 1.31$
$P_{tj}/P_b = 2.78$ $d_j^* = 0.144$ IN.

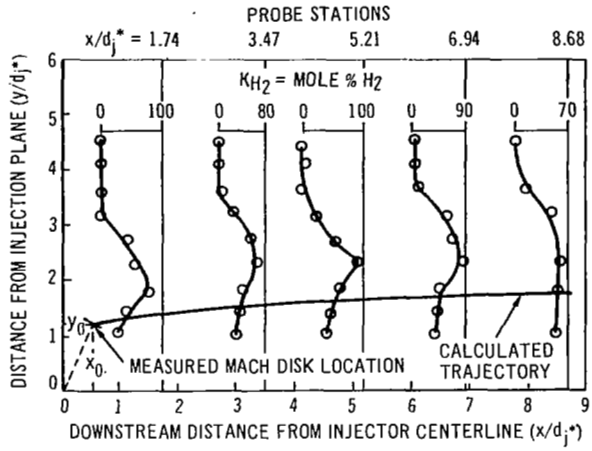

(b) $P_j/P_b = 1.00$ $q_j/q_a = 1.98$ $M_j = 1.5$
$P_{tj}/P_b = 3.67$ $d_j^* = 0.137$ IN.

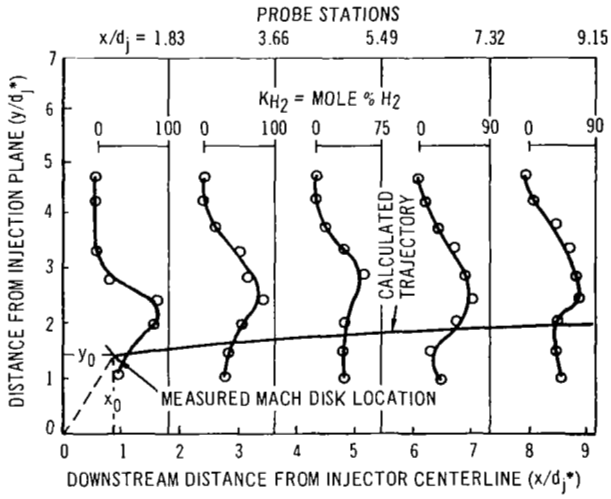

(c) $P_j/P_b = 1.00$ $q_j/q_a = 2.43$ $M_j = 1.67$
$P_{tj}/P_b = 5.17$ $d_j^* = 0.112$ IN.

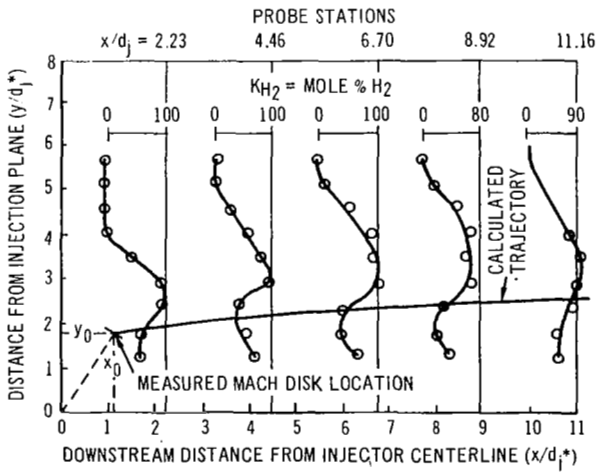

Fig. 10 JET TRAJECTORY AND INJECTANT CONCENTRATION PROFILES FOR SUPERSONIC INJECTION

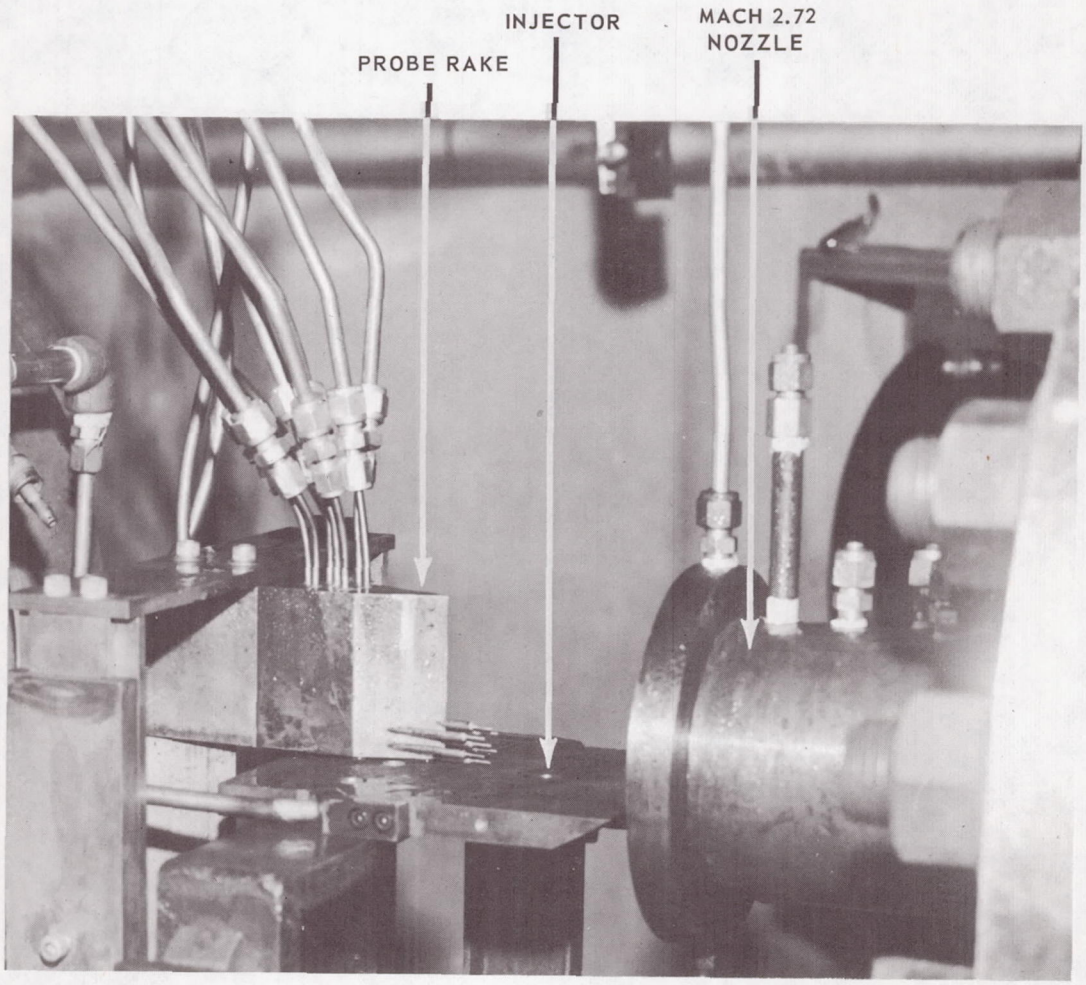

Fig. 11 FLAT PLATE INJECTOR WITH THREE DIRECTIONAL MOVEABLE PROBE

equipment made it possible to attain a reproducibility of ± 1% in hydrogen concentration by use of the integrated-signal analysis.[23] This excellent repeatability is attributed partly to the precise matching of the flow in the two branches of the gas chromatograph, which was achieved by maintaining pressure regulation on double sonic orifices in each circuit. Another factor in the improvement was the use of electrical integration of the output from the thermal conductivity cell rather than ratios of peak heights.

Figure 12 shows schlieren photographs of the penetration from the three injector configurations. The size of boundary layer separation increased as the disturbance in the main stream caused by the frontal area of the secondary jet increased. With the long axis of the rectangular nozzle aligned with the mainstream flow (Fig. 12a), the ratio of the separation height to the diameter of the circular injector (b/d_j) was 0.35. The values of b/d_j for the circular nozzle (Fig. 12b) and for the rectangular nozzle (where d_j is now the diameter of a circle of equivalent area perpendicular to the main stream, Fig. 12c) were 0.56 and 0.70, respectively. The jet structure was also altered by the shape of the injector, with the jet from the low-aspect-ratio injector (Fig. 12a) being the most deformed.

Figure 13 is a normalized scaled sketch of the fine jet structure deduced from each of the cases shown in Fig. 12. Although the shape of the injector strongly affects the shape of the fine structure of the underexpanded secondary jet (Figs. 12 and 13), it does not appear that the use of low-aspect-ratio injectors will improve penetration. As shown by Fig. 13, the location of the normal shock in the jet (called the "Mach disk" for the circular case) and the penetration in the near-downstream region were practically the same for the three injector shapes tested.

Figure 14 shows the measured hydrogen concentration contours at a downstream location of $x/d_j = 5$. Except for minor variations in the contours there is very little difference in the jet penetration and lateral spreading in the near downstream region.

The parametric variation of injectant pressure and Mach number established that the normal distance to the center of the Mach disk, or normal shock, in the secondary jet was a function of the jet-to-free-stream pressure ratio, which specified the degrees of underexpansion of the secondary jet. The initial drag on the secondary jet, which will be determined by the injector shape, will affect the downstream displacement of the Mach disk and the ratio y_0/x_0. The experiments substantiate the argument that the injector shape will affect the shape of the secondary jet structure and the orientation of the Mach disk, but the normal location of the Mach disk, and thus the penetration in the near downstream region are not greatly influenced by the injector shape. Furthermore, since the loss of jet momentum $\rho_j u_j^2$ across the normal shock is great, the orientation of the Mach disk and the direction

P_{t_j} = 68 PSIA

M_a = 2.1

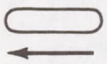

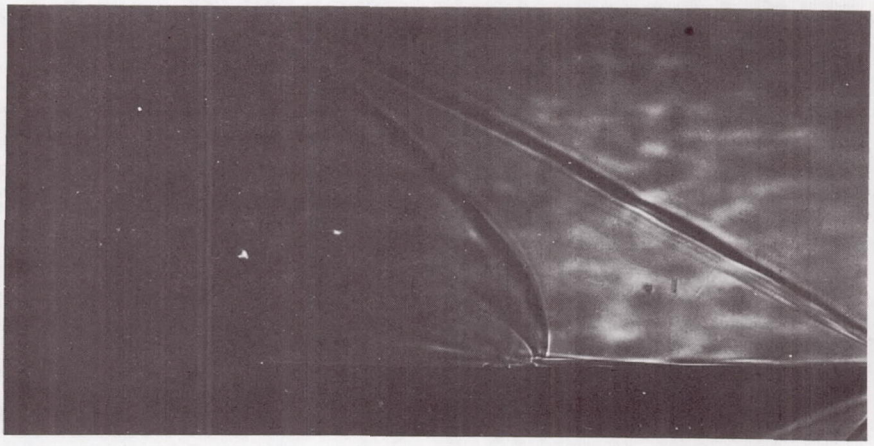

a. 1/4" x 1/16" SLOT (LONG AXIS ALIGNED WITH MAIN STREAM)

P_{t_j} = 67 PSIA

M_a = 2.1

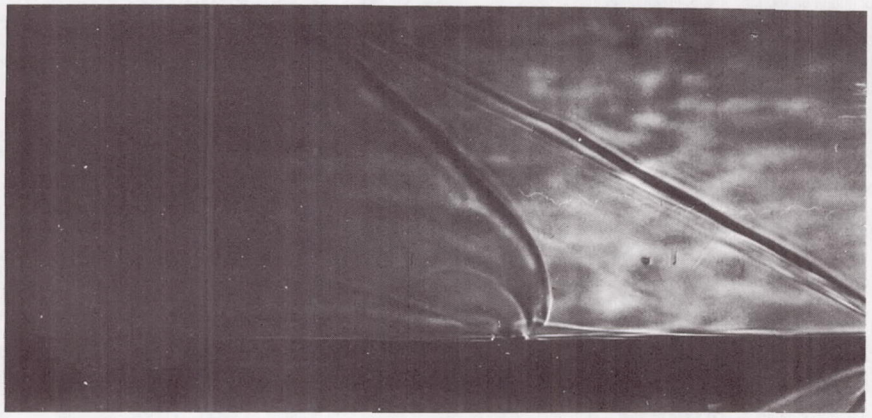

b. 0.136 INCH DIAMETER (CIRCULAR NOZZLE)

P_{t_j} = 65 PSIA

M_a = 2.1

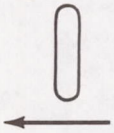

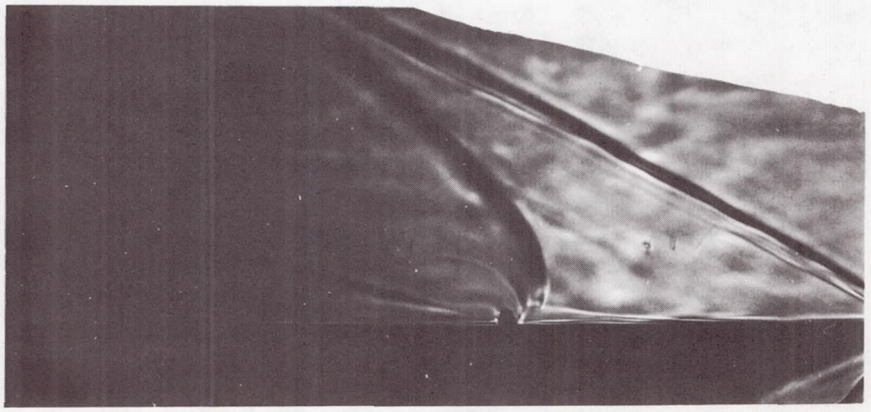

c. 1/4" x 1/16" SLOT (LONG AXIS PERPENDICULAR TO MAIN STREAM)

Fig. 12 SCHLIEREN PHOTOGRAPHS OF FINE JET STRUCTURE OF UNDEREXPANDED SONIC JETS (P_j/P_b = 5.23) IN A MACH 2.1 STREAM

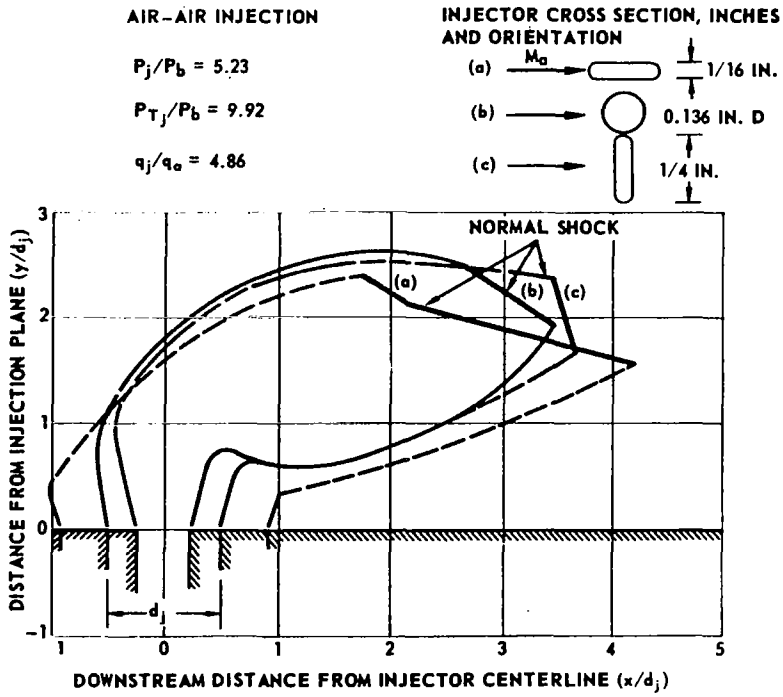

Fig. 13 EFFECT OF INJECTOR SHAPE ON JET STRUCTURE FOR UNDER-EXPANDED SONIC INJECTION INTO A MACH 2.1 SUPERSONIC STREAM

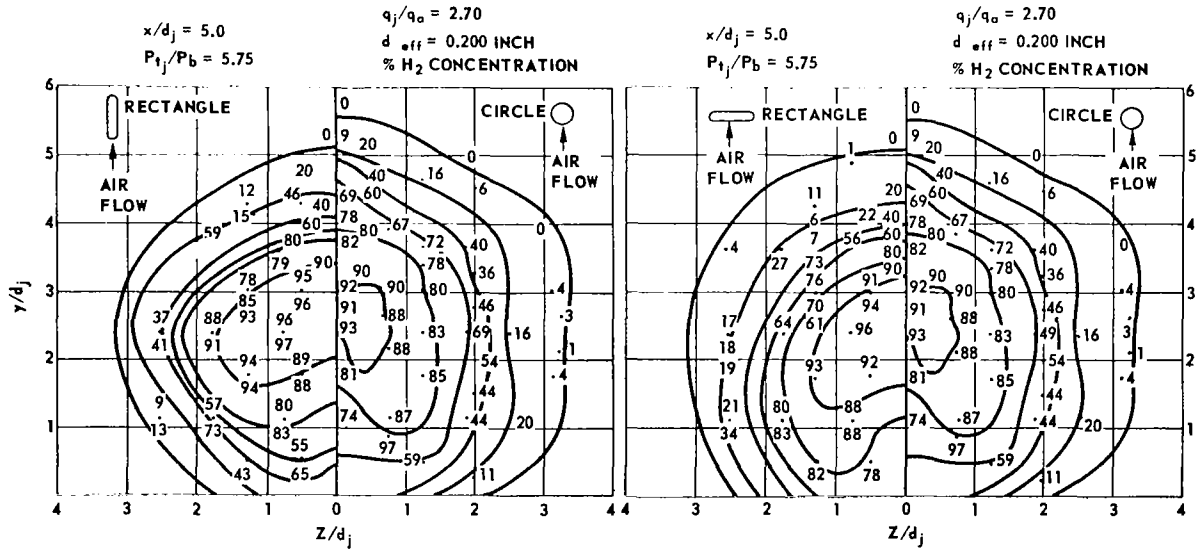

a. COMPARISON OF LONGITUDINAL SLOT AND ROUND HOLE

b. COMPARISON OF TRANSVERSE SLOT AND ROUND HOLE

Fig. 14 CONCENTRATION PROFILES FOR UNDEREXPANDED SONIC INJECTION INTO A MACH 2.7 STREAM.

of the jet as it crosses the shock also have little effect on the additional downstream penetration of the jet as a whole.

COMPARISON OF THEORY WITH EXPERIMENTAL RESULTS

To verify the trajectory theory, trajectories calculated by using Eq. (11) were compared with the experimentally determined concentration curves. For the case of matched pressure injection, q_j was evaluated at the point of injection and $\alpha_j = 90^\circ$. The integral was evaluated using Fig. 2 (it can also be done numerically) for 15° increments, and the trajectory was determined by evaluating the $\Delta\bar{s}$ from increment to increment until the full range of 90° was covered.

Because there was a relatively large separated boundary layer, the accuracy of the calculated trajectory rests heavily on the knowledge of the drag in that region. Although the details of the separated region were not precisely defined, it was assumed that the drag on the secondary jet can be approximated by the drag in the separated boundary layer of supersonic flow around a solid cylinder on a flat plate, and an estimate of C_D for the jet was calculated from the cylindrical surface pressure data presented in Ref. 22. The assumption that the drag on the fluid jet was equal to the drag on a solid cylinder resulted in a trajectory that was slightly below the experimentally determined maximum concentration locations (Fig. 8). However, in the absence of more definitive data on the interaction of the jet and the separated flow, it is suitable for a conservative estimate of the jet trajectory. In the more practical cases of jet penetration, such as the design of a fuel injector, it may not be possible to measure the separation height. Therefore, a calculation that estimates the effect of the separated boundary layer on the trajectory of the jet but is based only on freestream conditions is desirable. To provide such a calculation, we compared C_D for the jet as it penetrated a distance equal to b in a stream with no boundary layer, $C_D = f(M_a, \alpha)$ as in the foregoing, and C_D for the separated zone. Since the drag for the jet in the freestream is larger than the drag in the separated boundary layer, the penetrations in the two cases can be made equal if the freestream trajectory is vertically displaced such that the freestream drag times the vertical distance over which it acts is equal to the separation zone drag times the separation height. For the experimental data shown in Fig. 8, the offset distance (for which $C_D = 0$) that was required to make the completely inviscid trajectory coincide with the trajectory shown was twice the compressible flow boundary-layer thickness as calculated by Pai[24] and Eckert and Drake.[25] Thus, in this procedure the trajectory for injection into a completely inviscid freestream is calculated, then it is displaced upward a vertical distance equal to twice the compressible flow boundary layer thickness.

To calculate the trajectory of an underexpanded jet, the location of the Mach disk (x_0, y_0) was determined from the experimental correlations. The normal displacement y_0 was taken directly from Fig. 7 and the ratio of normal to downstream displacement $y_0/x_0 = 1$, was used in accordance with the data from Refs. 13 and 21 shown in Fig. 15. The total displacement z , was calculated from the assumption

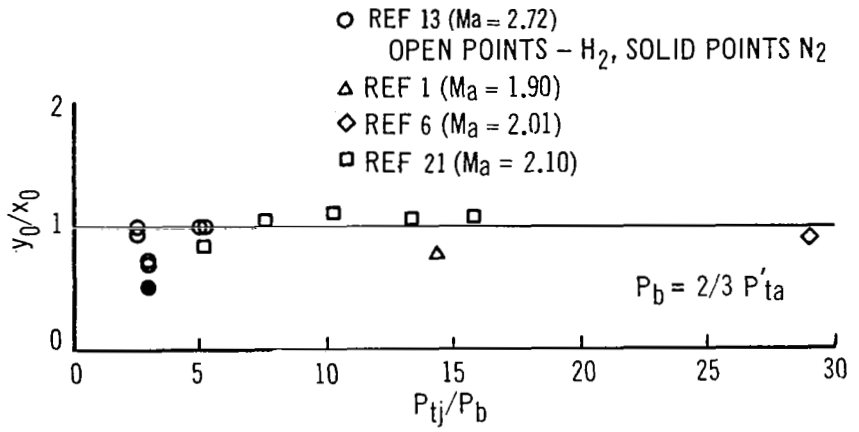

Fig. 15 RATIO OF PERPENDICULAR TO LONGITUDINAL MACH DISK DISTANCE VERSUS RATIO OF TOTAL INJECTANT PRESSURE TO EFFECTIVE BACK PRESSURE

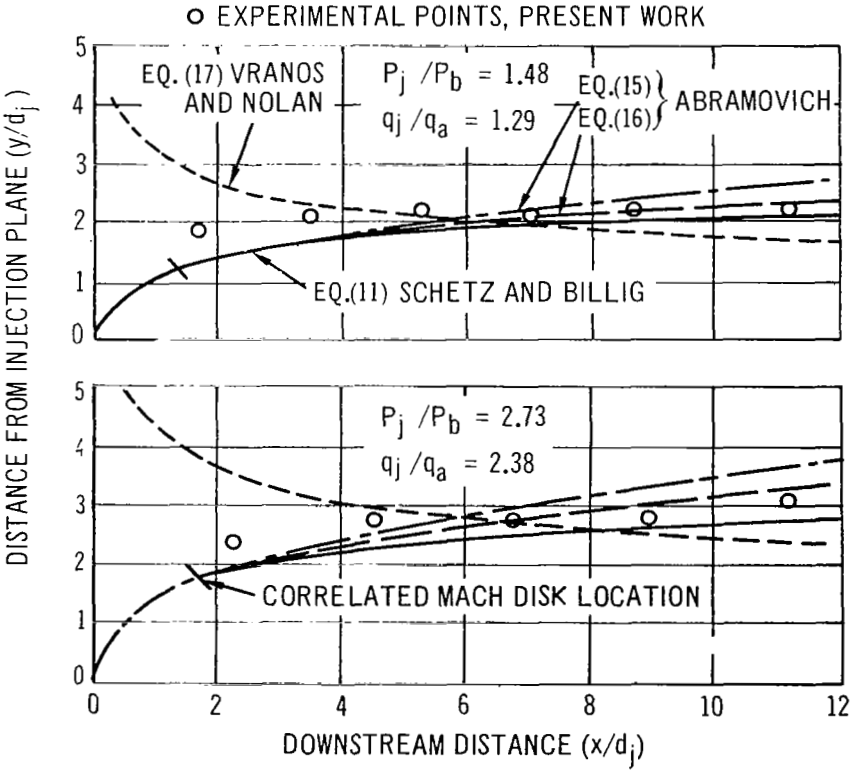

Fig. 16 MAXIMUM CONCENTRATION LOCUS FOR SONIC H_2 INJECTION INTO MACH 2.72 AIR STREAM, COMPARISON OF DATA WITH VARIOUS EQUATIONS

$$z = (x_0^2 + y_0^2)^{\frac{1}{2}} \tag{13}$$

The Mach number upstream of the Mach disk was calculated from

$$\frac{z}{d_j^*} = M_j^{1/(\gamma_j-1)}\left[\left(\frac{\gamma_j-1}{2}\right)^{\gamma_j/(\gamma_j-1)}\left(\frac{\gamma_j+1}{4.8\gamma_j}\right)^{\frac{1}{2}}\right] \tag{14}$$

With this Mach number, q on the downstream side of the Mach disk was calculated from the normal shock equations, then the jet trajectory downstream of the Mach disk was calculated from Eq. (11). The procedure for calculating the trajectories of the supersonic jets was the same, except that the actual measured values of x_0 and y_0 were used, and the length of the supersonic portion of the nozzle was included in y_0.

The trajectories for underexpanded jets calculated on this basis are characterized by a rapid penetration to a point where the Mach disk occurs and sharply reduces q, followed by a gradual increase in penetration that occurs downstream of the Mach disk is due to the low value of q/q_a in this region.

The location of the Mach disk and the resulting loss of energy is a strong function of P_{tj}/P_b. The method of calculating the trajectory for underexpanded jets and supersonic jets downstream from the Mach disk rests heavily on the previously described extension of the correlation of z vs M_j (Eq. 14) in the quiescent medium to the case having external flow. Instream pitot and static pressure measurements in the region of the Mack disk are needed to ascertain the validity of this method.

Comparison of Some Penetration Correlations

Two types of expressions for jet penetration were found, one based on the trajectory of maximum injectant concentration, and the other based on the trace of the outer boundary of the jet. Equation (11) and the following equations (15-17) are of the former type, whereas Eq. (18) is of the latter type. Figures 16 and 17 compare these correlations with data from two of our tests with underexpanded hydrogen injection into a Mach 2.72 airstream. Thus

$$y/d_j = [(q_j/q_a)\ x/d_j]^{0.394} \qquad \text{(Ref. 8)} \tag{15}$$

$$y/d_j = (q_j/q_a)^{0.434}(x/d_j)^{0.333} \qquad \text{(Ref. 8)} \tag{16}$$

$$y/d_j = 1.64\ [q_j M_a/q_a M_j)\cos^2\alpha_j]^{0.533}(x/d_j)^{-0.259} \qquad \text{(Ref. 9)} \tag{17}$$

$$\tilde{y}/d_j = 1.68\ [q_j M_a/q_a M_j)\cos^2\alpha_j]^{0.5}(x/d_j)^{0.0866} \qquad \text{(Ref. 9)} \tag{18}$$

Equations (15) and (16), which were developed for a subsonic main flow,[8] agree reasonably well with the experimental values for $x/d_j \leq 8$ but lead to unreasonably large penetrations farther downstream. The values of the exponent on (q_j/q_a) in these formulas are satisfactory for supersonic flow (shown by the correspondence of the trajectories at $x/d_j = 1.0$), but the values of the exponent on (x/d_j) are too high; they predict the slowly increasing penetration typical of subsonic flow rather than the rapid penetration, quick turning, and flat trajectory of the secondary jet in a supersonic freestream.

Equation (17) also was based on data far downstream, ($x/d_j^* = 7.5$ to 72). The negative exponent on (x/d_j^*) attempts to account for the unsymmetric mixing that occurs in this far downstream region and causes the maximum concentration to shift toward the flat plate. The correlation is unrealistic for $x/d_j^* < 6$.

Only Eq. (11) considers the degree of underexpansion as well as q_j/q_a. Of the four correlations it appears to describe best the location of the maximum concentration trajectory. Furthermore, because the structure of the emergent jet is considered, it is the most realistic.

The location of the jet boundary or maximum penetration is partly a matter of definition. Vranos and Nolan[9] defined the jet boundary as the y/d_j^* value at which the mole fraction of the injectant is 0.005, and they used this definition in the development of Eq. (18). Another definition of the boundary is the y/d_j^* value at which the mole fraction has fallen to 10-20% of the peak value at the same x/d_j^* in the plane of the jet centerline. The latter definition was more convenient for determining the jet boundary from the experimental concentration curves in the present work (Fig. 8-10). Compatibility between the two definitions is shown by the agreement between the jet boundary as calculated with Eq. (18) and the experimental values based on the latter criterion for H_2 injection into a Mach 2.72 airstream (Fig. 17).

Since the foregoing comparisons have been concerned with the relative locations of the maximum concentration (y/d_j) and the outer jet boundary $(\tilde{y}/d_j)$, it is now important to examine the effect of q_j/q_a and the degree of underexpansion on the absolute penetration. The importance of evaluating injectors on this basis is that when the mass flow of the injector is specified, as by a required fuel equivalence ratio for example, the better injector will be the one that gives the greatest fuel penetration. As shown in Table 1 the effect of underexpansion, or increased injectant pressure, on the absolute penetration is small. When the injection pressure is increased by a factor of 2.73 relative to the matched-pressure case, the increase in absolute penetration based on maximum concentration (y) is only 7 or 8%. This small increase in the absolute penetration of the maximum concentration is due to the unsymmetrical mixing of the injectant and the freestream which occurs closer to the injector for higher degrees of underexpansion. For fuel injectors this phenomenon may indeed be beneficial, because the fuel would be coming into more intimate contact with the air, resulting in more rapid ignition. Since this is due to co-current

Table 1

Effect of Injection Pressure on Absolute Penetration Measured at x = 1.0 In.

p_j/p_b	d_j, in.	x/d_j	y, in.	$\tilde{y}$, in.
0.75	0.204	4.90	0.286	0.530
1.48	0.144	6.94	0.288	0.518
2.73	0.112	8.92	0.308	0.588

mixing, a quantitative evaluation of this effect is beyond the scope of this work. Comparison of the outer jet boundaries ($\tilde{y}$) in Table 1 shows a 10% increase in penetration for $P_j/P_b = 2.73$. For either y or $\tilde{y}$, an increase in P_j/P_b from 0.75 to 1.48 had no appreciable effect. The general conclusion from Table 1 is that placing a large demand on a fuel pressurization or pumping system to increase fuel pressure for sonic injection will have only a small payoff.

SUPERSONIC INJECTION

One clear result of the analytical and experimental studies presented here and also from previously reported experimental studies is the obvious importance of q_j/q_a on penetration. Although increasing P_{tj} increases this ratio, the effects are not large for P_{tj} below the pressure match and are quite small for underexpanded injection. Accepting the result that P_j should be the matched pressure so that a relatively shock-free jet flow occurs, then it is instructive to explore another possibility for increasing q_j/q_a and hence penetration, viz., varying M_j. Since $q = \rho\gamma M^2/2$, increasing M_j has the desired effect of increasing q_j for the same static pressure level.

Equation (11) can be presented in the same form as Eqs. (15)-(17) as shown below:

$$y/d_j^* = [(q_j/q_a)(x/d_j^*)]^{0.4} \tag{19}$$

Consider the penetration of a given amount of fluid per unit time by normal, sonic injection into a supersonic airstream. One can write $q_j = \rho_j u_j^2/2 = \dot{m}u_j/2A_j$. Take as the standard for comparison a case with $P_j = P_b$. As opposed to this, take a supersonic case, denoted by subscript s, with an injection pressure $P_j = P_b$. Now using Eq. (19), y_s/y, at a given distance $\tilde{\tilde{x}}$ downstream of the injection station, can be determined as

$$\frac{(y/d_j)_s}{(y/d_j^*)} = \frac{(q_j/q_a)_s\ (\tilde{\tilde{x}}/d_j)_s}{(q_j^*/q_a)\ (\tilde{\tilde{x}}/d_j^*)}^{0.4} \tag{19a}$$

With $\tilde{\tilde{x}} = \tilde{\tilde{x}}_s$ and $q_a = q_{as}$, this becomes

$$y_s/y = (d_{js}/d_j^*)^{0.6}\ (q_{js}/q_j^*)^{0.4} \tag{20}$$

We can now assess the magnitude of any advantage to be gained. First, however, we must determine $d_j(M_j)$ for a constant mass flow and fixed P_j. Using

$$\rho = \rho_j^*(1 + M^2/5)^{-5/2} \qquad a = a_j^*(1 + M^2/5)^{\frac{1}{2}} \tag{21}$$

it can be shown that

$$A_s/A^* = \xi^{0.5} M^{-1} \tag{22}$$

where $\xi \equiv 1.2/(1 + 0.2M^2)$. Taking sonic injection as the standard case

$$(d_{js}/d_j^*)^{0.6} = \xi^{0.15} M^{-0.3} \tag{23}$$

giving finally

$$y_s/y = \xi^{0.15} M^{0.5} \tag{24}$$

Figure 17 shows that experimental values of y_s/y, the ratio of the peak concentration from supersonic injection to that for matched-pressure sonic injection, are in good agreement with the theoretical effect predicted for the particular case of matching of mass flow and static pressure at the injector exit. For $M_{js} = 1.67$, the increase in penetration is 25% ($y_s/y = 1.25$). Since an increase M_{js} for a matched-pressure jet must be paid for by increasing P_{tj} and since, as earlier stated, a more appropriate matching parameter of transverse supersonic streams is the static pressure behind strong disturbances in both streams, a comparison of the penetration of supersonic and sonic jets with equal P_{tj} and $\dot{m}_j$ was made (Fig. 18). With these restrictions on the theoretical relationship, theoretical penetration gain peaks at $M_j = (5)^{\frac{1}{2}}$. Unfortunately, the data scatter for this plot is large, and the variations in measured penetration ratios at different downstream locations show no discernible pattern, so that further experimentation is needed to verify the theory. However, Figs. 17 and 18 do show a gain in penetration with supersonic injection.

INTERACTION SHOCK SHAPE FOR TRANSVERSE INJECTION

The effects of injector shape on jet penetration were further explored by studying the interaction shock shapes produced by jets from differently shaped orifices. Previous attempts by others (e.g., Refs. 26 through 28) to predict the shape of the interaction shock accompanying transverse injection across a uniform supersonic stream have been based on the concept of some "equivalent solid body," using results for shock shapes past blunt bodies. References 26 through 28 used the well-known blast-wave theory. The blast-wave theory is simple and convenient to apply, but suffers from the disadvantages that it cannot predict the shock stand-off distance and does not, in general, provide very good estimates of shock shapes past solid bodies. Recently, very simple expressions for shock shape and stand-off distance for blunt bodies have been shown to provide excellent predictions of both quantities (Ref. 29).

The concept of an "equivalent solid body" is used in conjunction with simple expressions for the shock shape around blunt solid bodies to predict shock shapes produced by transverse injection into a supersonic stream. To apply the shock shape expression (Ref. 29) it is necessary to determine some equivalent for the solid body nose radius in the transverse jet case. The one length scale that is directly known

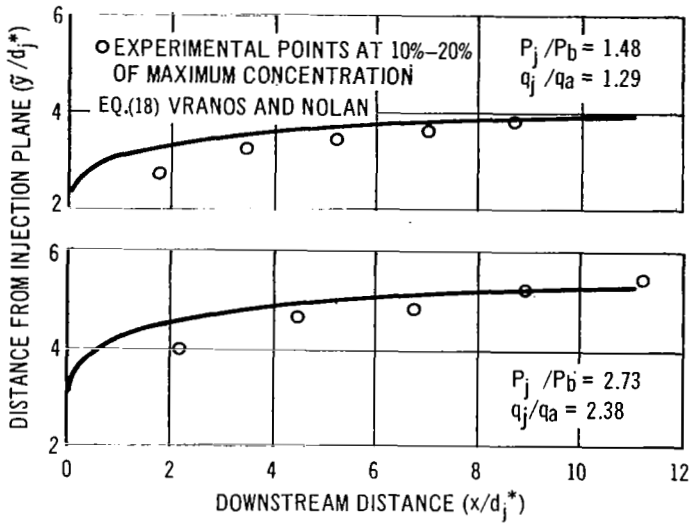

Fig. 17 JET BOUNDARY FOR H_2 INJECTION INTO MACH 2.72 AIR STREAM COMPARISON OF DATA WITH EQ. (18)

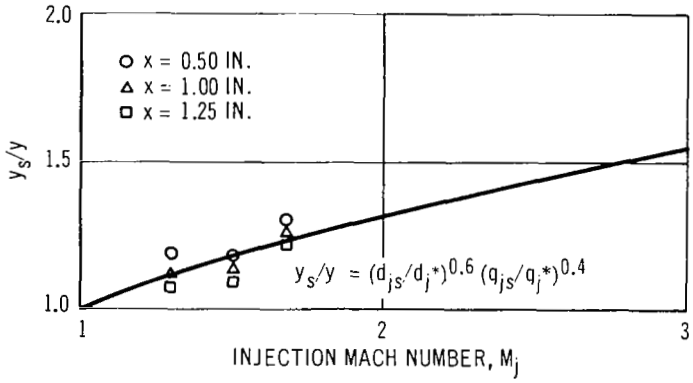

a. CONSTANT P_{js} AND $\dot{m}_{js}$

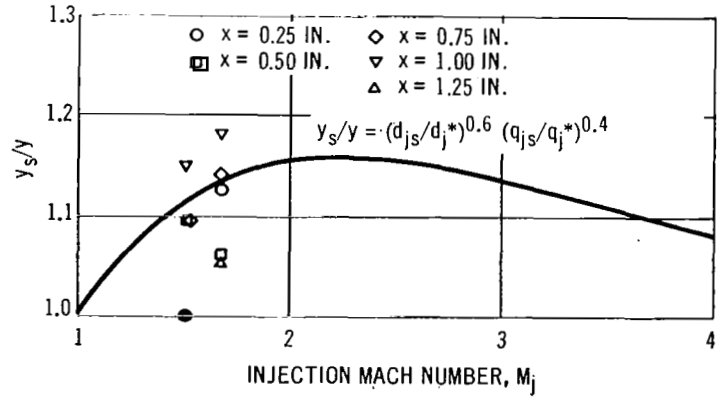

b. CONSTANT P_{tjs} AND $\dot{m}_{js}$

Fig. 18 MEASURED PENETRATION (y_s/y) AT VARIOUS DOWNSTREAM LOCATIONS FOR 10° CONICAL SUPERSONIC INJECTORS

is the radius of the injection port. The injection port radius by itself is not, however, a suitable choice for the "body" nose radius as it does not measure the size of the obstruction presented to the main flow. One can simply employ the equivalent nose radius given by the blast wave theory, i.e.,

$$R_{B_1} \equiv \left(\frac{\dot{m}_j}{\rho_a u_a} \right)^{\frac{1}{2}} \tag{25}$$

with the shock shape formula of Ref. 29. An alternative approach can be developed based on the work of Refs. (12), (21) and (30). Here the height of the Mach disk, h, can be chosen as a measure of the obstruction and used as the "body" radius. From the results of the cited references, a simple formula for this height may be written for cases with $\gamma_j = 1.4$:

$$h \equiv R_{B_2} = (2r_j)\ K(M_j) \left(\frac{P_j}{P_b} \right)^{\frac{1}{2}} \tag{26}$$

where $K = 1.0$ for $M_j = 1.0$. Both possible choices (Eq. (25) and Eq. (26)) will be tested by comparison with experiment.

With these results, the formula of Ref. 29 applied to the present problem can be written:

$$\frac{x}{r_j} = \frac{R_B}{r_j} + \left(\frac{\Delta}{R_B} \right) \left(\frac{R_B}{r_j} \right) - \left(\frac{R}{R_B} \right) \left(\frac{R_B}{r_j} \right) \text{ctn}^2\ (\theta)$$

$$= \left\{ \left[1 + \left(\frac{y}{r_j} \right)^2 \left(\frac{r_j}{R_B} \right)^2 \left(\frac{R_B}{R} \right)^2 \tan^2\ \theta \right]^{\frac{1}{2}} - 1 \right\}, \tag{27}$$

where Δ/R_B is the nondimensional stand-off distance given as

$$\Delta/R_B = 0.143 \exp\ [3.24/M_a^2], \tag{28}$$

and R/R_B is the nondimensional radius of curvature of the shock at the nose

$$R/R_B = 1.143 \exp\ [0.54/(M_a - 1)^{1.2}] \tag{29}$$

Observations of schlieren photographs (Ref. 6 and Fig. 12) of transverse jet injection show that the interaction shock has an inflection point that is displaced above the solid surface. This can be interpreted to mean that the nose of the "equivalent solid body" is located above the surface. A good prediction of this displacement is necessary to provide an accurate picture of the shock shape in the near field. The displaced height of the inflection point is denoted as β, and it has been possible to correlate this height, when nondimensionalized, with the non-dimensional equivalent body radius, i.e., β/r_j vs. R_{B_2}/r_j, as can be seen in Fig. 19.

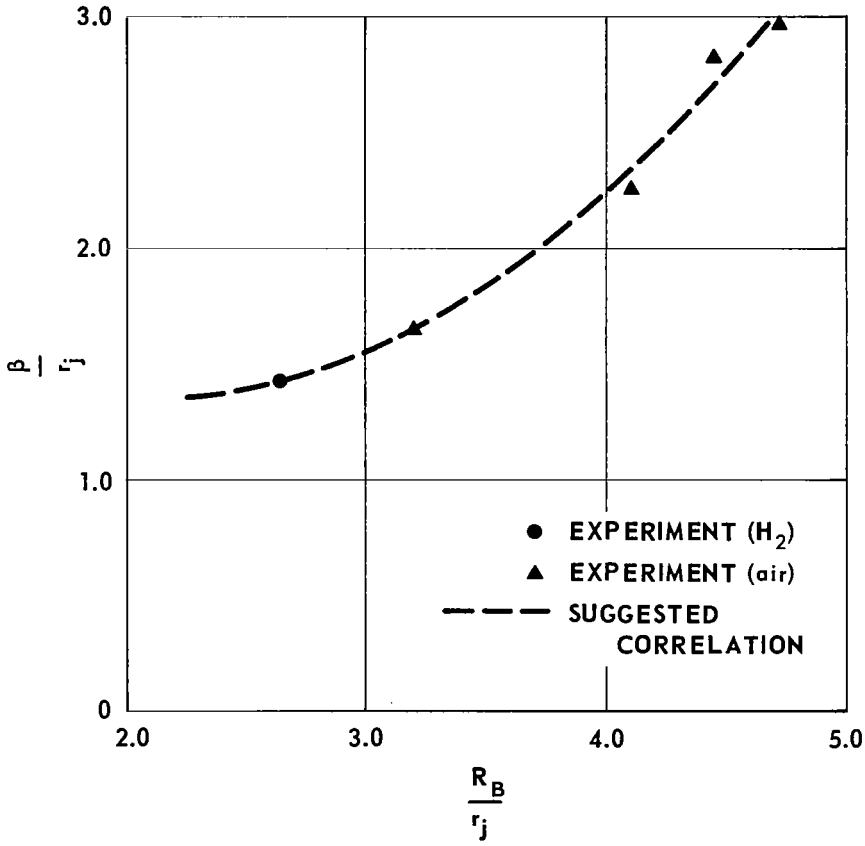

Fig. 19 SHOCK WAVE DISPLACEMENT CORRELATION

The predictions of this analysis have been compared to experimental results for the following three cases shown in Figs. 20 through 22, respectively: (a) sonic air injection through a round hole into a Mach 2.1 air stream; (b) sonic H_2 injection through a round hole into a Mach 2.7 air stream; and (c) sonic air injection with a 4 by 1 slot aligned with and across a Mach 2.1 air stream. Agreement is reasonably good in all cases, with the "body" radius of Eq. (26) providing a better prediction, especially for the hydrogen injection case. A result of significant practical importance emerges from this study. The analysis predicts that the shock shape is not a function of injector port shape; this is confirmed by experiment as seen in Fig. 22. It is important to note, however, that the experiments permitted only the planform of the interaction shock to be determined. Some difference in shock shape in planes other than that including the jet trajectory might exist, but would go undetected here. Nevertheless, the fact that the planform of the shock shape is insensitive to injector port shape is significant and adds further evidence to the conclusion that jet penetration is only weakly dependent on injector shape.

APPLICATION TO SCRAMJET DESIGN

At this point, it is informative to study the design problem of fuel injection in the combustion chamber of a hypersonic ramjet. Take a typical case as a $q_\infty = 5000$ psi trajectory with a velocity decrement from freestream to combustor inlet of 1500 fps and an inlet kinetic energy efficiency of 97%. Consider gaseous hydrogen with a total temperature of 294°K as the fuel, and take stoichiometric proportions of fuel and air. Let us investigate a flight Mach number of 6.0. For this case, an $\eta_{KE} = 0.97$ translates to a total pressure recovery of 51%. The 1500-fps velocity decrement gives a combustor Mach number of 2.2, and this results in a combustor stagnation pressure of 1107 psia, a static pressure of 104 psia, $q_a = 351$ psi, and $(P_{ta}') = 695$ psia. Estimating that "matched" pressure injection will occur, for sonic injection, at $P_j = \frac{2}{3}(P_{ta}')$ gives $P_j = 464$ psia, and $q_j = (\gamma/2)\,(1)\,(464) = 325$ psi. Thus, $q_j / q_a = 325/351 = 0.925$.

For a circular combustion chamber of diameter D (ft), the air mass flow is 595 D^2 lb/sec. For stoichiometric hydrogen in air (0.0292 lb H_2/lb air) and n round injection holes of diameter d_j, there results

$$(0.0292)(595\ D^2) = n(0.14)P_{t_j}(\pi d_j^2/4)(144)T_{t_j}^{\frac{1}{2}} \qquad (30)$$

or $d_j/D = 0.062$ for $n = 10$. If we now select some axial distance downstream from the injection station, the fuel penetration can be displayed on a cross-section of the combustion chamber. Noting that for $q_j/q_a \approx 1$, as in this case, the total fuel penetration is achieved in a short distance downstream (see Fig. 8), we select $x = 4\ d_j$ as the axial station for display (open circles in Fig. 23a). (No attempt to show the distortion of the jet cross section has been made.) The striking result is that rather poor coverage of the air flow in the combustor has been achieved, and a low combustion efficiency would surely result. Therefore, one looks to see how this situation can be improved. Since the penetration is a function of the

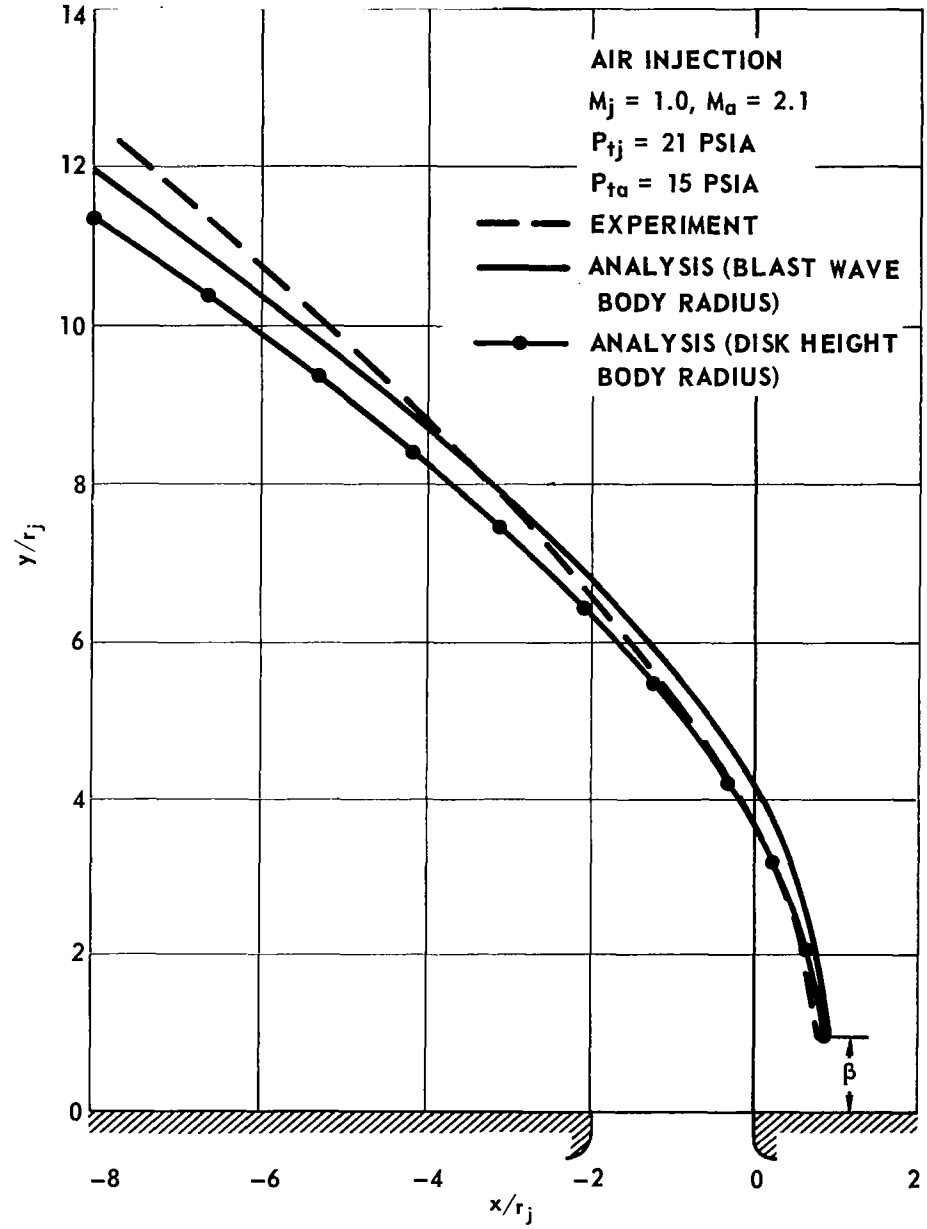

Fig. 20 SHOCK SHAPE FOR SONIC AIR INJECTION

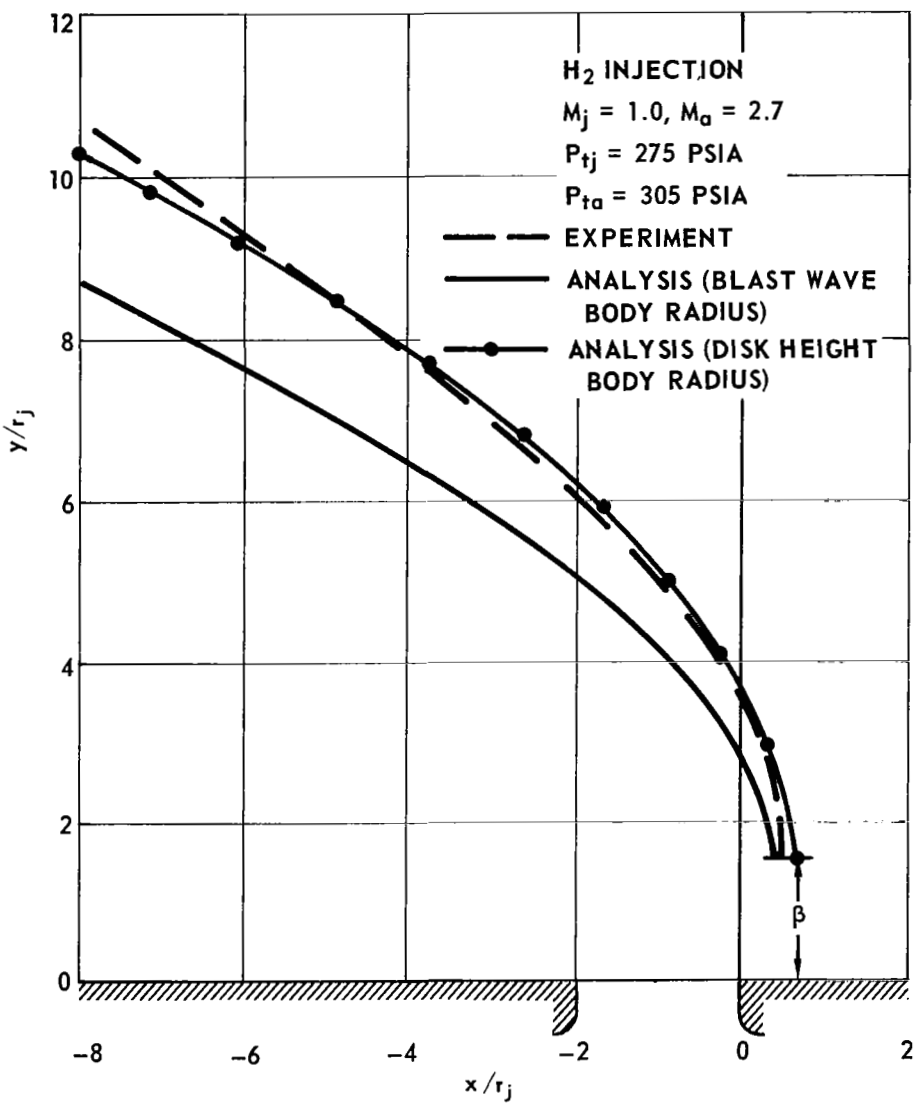

Fig. 21 SHOCK SHAPE FOR SONIC HYDROGEN INJECTION

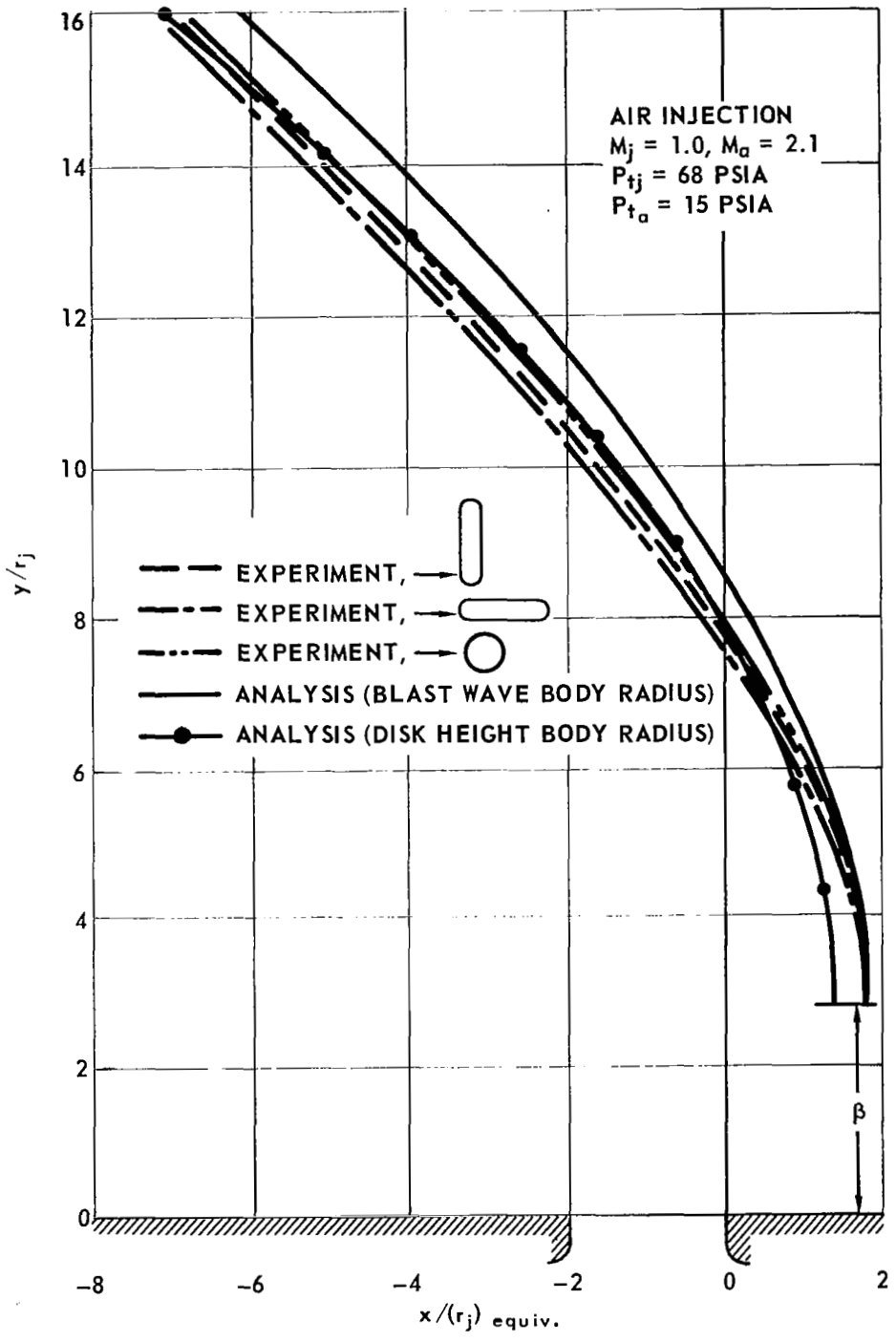

Fig. 22 SHOCK SHAPES FOR VARIOUS SHAPES OF INJECTION PORT

initial hole size and the hole size varies with the number of injectors, it would seem profitable to reduce the number of injectors. The results achieved by reducing the number of injectors from 10 to 4 are shown as open circles in Fig. 23b. Indeed, the fuel does penetrate somewhat farther into the air stream; however, larger air gaps are left around the periphery, and one could say that the coverage of the air stream is, if anything, poorer in this case than with the 10-hole injector.

It is instructive to consider briefly the effect of the choice of fuel on this question. Consider propane (C_3H_8), which has a molecular weight of 44, a ratio of specific heats of 1.16, and stoichiometric fuel-air ratio of 0.064. The calculated d_j/D is 0.044 for 10 holes and stoichiometric injection. Furthermore, the momentum ratio will be less than for hydrogen injection. Thus, since the initial diameter and the momentum ratio are both reduced, the penetration pattern for propane would be distinctly worse than that for hydrogen. The low density of hydrogen is, therefore, a real advantage with regard to penetration, since it keeps the initial jet diameter large.

Returning now to hydrogen and noting the results of Table 1, it can be seen that some advantage can be gained by over-pressuring the jet. It does not, however, appear profitable to consider a pressure ratio greater than 2.0, since the gain in penetration diminishes rapidly, and P_{tj} at an overpressure of 2.0 is already 1758 psia. The penetration pattern obtained in this way is shown as solid circles in Figs. 23a and 23b. Although this is certainly an improvement, the 10-hole injector is still superior, and the pattern still leaves much to be desired. We saw in Figs. 18a and 18b that some gain in penetration could be obtained by supersonic injection but even these gains are not too significant. For example, if $P_{js} = P_j = 464$ psia and $\dot{m}_{js} = \dot{m}_j$ but M_j is increased to 2, the penetration would increase by about 30% (Fig. 18a), but the required P_{tjs} would increase from 878 psia to 3630 psia. On the other hand if we put the more reasonable constraint of $P_{tjs} = P_{tj} = 878$ psia with $\dot{m}_{js} = \dot{m}_j$ and let $M_j = 2$ then the increase is but 15% (Fig. 18b). Another factor that could have some effect on the fuel-air contact is the ratio of d_{js}/d_j. For $P_{js} = P_j$ this ratio decreases with increasing M_j and is equal to 0.639 at $M_j = 2$ which probably is detrimental to mixing. On the other hand for $P_{tjs} = P_{tj}$ the ratio d_{js}/d_j increases with increasing M_j and is equal to 1.30 at $M_j = 2$.

One means of improving the over-all penetration pattern is to alter the shape of the combustion chamber itself. Figure 23c shows an elliptical (3:1) cross section of the same area as the circular cross section. Only the points corresponding to an overpressured jet are shown. Clearly, a much better fuel distribution is obtained in this way. (One disadvantage of this change is a 23% increase in the surface area of the combustor and thus an increase in heat transfer and skin-friction drag.)

Now let us look at flight Mach number of 10 on the trajectory described previously. Here $\eta_{ke} = 97\%$ gives a pressure recovery of 19%. We further get $M_a = 3.9$ and $q_j/q_a = 0.67$. Matched pressure injection gives $P_{tj} = 750$ psia. For stoichiometric proportions, 10 holes require $d_j/D = 0.042$. If we envision the same combustor operating at both the

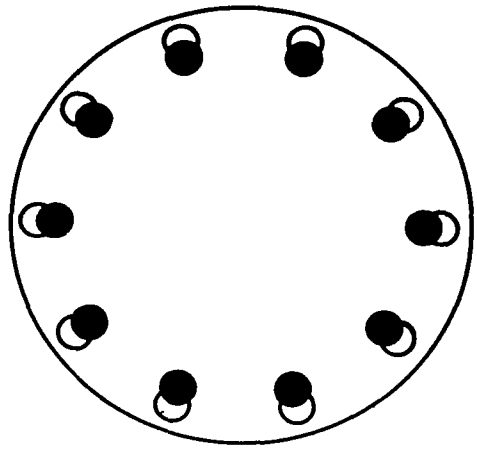

$P_{t'_j}/P_{t_j}$

1 ○

2 ●

$\frac{x}{D} = 0.25$

$\frac{x}{d_j} = 4.0$

a. CIRCULAR, TEN HOLES

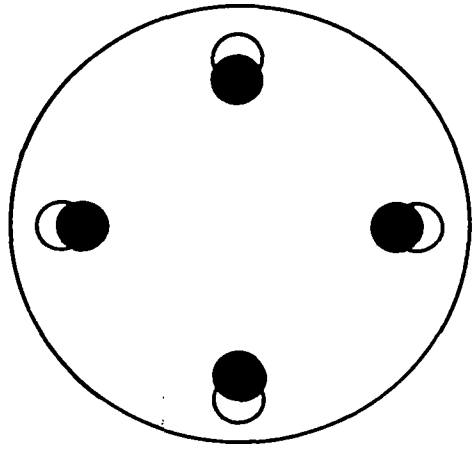

$P_{t'_j}/P_{t_j}$

1 ○

2 ●

$\frac{x}{D} = 0.25$

$\frac{x}{d_j} = 2.53$

b. CIRCULAR, FOUR HOLES

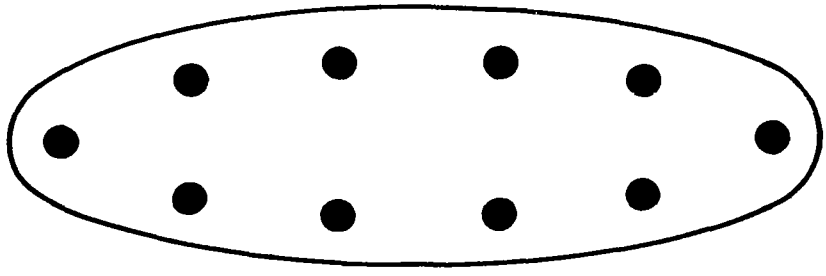

$P_{t'_j}/P_{t_j} = 2$

$\frac{x}{D_{eff}} = 0.25$

$\frac{x}{d_j} = 4.0$

c. ELLIPTICAL (3:1), TEN HOLES

Fig. 23 COMBUSTION CHAMBERS FOR MACH 6 FLIGHT OF A SCRAMJET WITH STOICHIOMETRIC HYDROGEN INJECTED

Mach 6 and Mach 10 flight conditions, then one could use only five of the holes at Mach 10. Since the diameter is then the same and q_j/q_a is very nearly the same for the Mach 10 case, the penetration pattern would be as shown in Fig. 23a or 23c using half of the holes.

Conclusions

From the experimental studies it can be concluded that, as assumed in the trajectory analysis, the downstream region where the injectant behaves as a discrete jet with negligible mixing is quite short ($x/d_j^* < 10$). To describe accurately the jet behavior of the injectant farther downstream, coaxial mixing must be taken into account.

The use of a "solid-body" drag model to describe the penetration of a fluid jet has been re-examined and extended to include the case of a supersonic external stream. A simple analysis was developed which relaxed most of the assumptions common to previous work. The most important step was the removal of the restrictive assumption that the normal component of the jet momentum is conserved. With this restriction removed, good agreement between the theory and experimental data was obtained using local values of the drag coefficient for an inclined cylinder. For underexpanded jets exhausting into the mainstream, the shock structure caused by underexpansion in the jet itself is the predominant factor governing penetration. Introduction of an "effective back pressure" enabled the development of a Mach disk correlation analogous to the well-documented but much simpler case of underexpanded jets exhausting into a quiescent atmosphere. With this correlation the conditions of the jet just downstream of the Mach disk can be approximated and the resulting trajectories, which agreed closely with experimental results, are calculated.

Several semiempirical penetration and trajectory correlations were compared with the experimental results obtained herein. They were based on other measurements taken far downstream ($10 < x/d_j^* < 70$). The trajectory calculation developed herein best described the location of the jet trajectory. With respect to the outer boundary of the fuel jet, the correlation by Vranos and Nolan agrees well with the near downstream data from the present studies.

While the nondimensionalized penetration (y/d_j) for sonic injection is governed by the degree of underexpansion and the initial ratio of jet-to-freestream momentum, variation in the absolute penetration due to underexpansion is small if jets with equal mass flow are compared. The analytical analysis indicated that result and the experimentally measured concentration centerline profiles and crossectional contours verified the conclusion. In fact, due to the losses involved as the underexpanded jet crossed the normal shock (Mach disk), the absolute penetration for a jet with the underexpansion ratio of 1.48 was not appreciably different (possibly even slightly less) than that of a jet whose injection pressure matched the effective back pressure of the supersonic freestream. A further increase to a 2.73 factor on underexpansion caused only an 8-10% gain in penetration. Thus, little is to be gained by increasing the injection pressure above the level of the effective

back pressure. Penetration can be increased by going to supersonic injection. A theoretical comparison of penetration from a supersonic jet and a sonic jet of the same total injectant pressure and mass flow showed a maximum penetration at $M_j = (5)^{1/2}$. The experimentally measured penetration at $M_j = 1.67$ was greater than that for $M_j = 1.50$ and in both cases it was 10 to 15% better than that for sonic injection. However, the scatter of the experimental points on this plot was large, and additional experimentation at higher values of M_j must be performed to verify that increasing M_j beyond $(5)^{1/2}$ does not improve penetration.

Absolute penetration is at best only weakly effected by injector hole shape. The momentum loss incurred by an underexpanded injectant as it crosses the Mach disk practically cancels any penetration differences caused by injector shape. Local concentration differences occur but these have little effect on the additional downstream penetration of the jet as a whole.

The secondary effects of injector shape on penetration were further emphasized by the development of an expression for the interaction shock shape. The concept of an "equivalent solid body" with radius equal to the Mach disk height gave good results when used in conjunction with simple expressions for the shock shapes around blunt bodies. The agreement between the calculated shock shapes and those from schlieren photographs of the interaction shock caused by transverse injection was excellent. Finally, the analysis has been applied to the question of the design of a fuel injection system for a supersonic combustion ramjet. Low q_j/q_a values are generally to be expected for real flight cases. Under these circumstances, some underexpansion of the fuel jets is desirable, but it was shown that the attainment of a roughly uniform fuel air ratio throughout the cross section of a circular duct by fuel jet penetration is unlikely.

REFERENCES

1. Morkovin, M. V., Pierce, C. A., Jr. and Craven, C. E.: Interaction of a Side Jet with a Supersonic Main Stream. Bull. 35, Engineering Research Institute, Univ. of Michigan (September 1952).

2. Ferrari, C.: Interference between a Jet Issuing Laterally From a Body and the Enveloping Supersonic Stream. Bumblebee Series Rept. 286, Applied Physics Lab., Johns Hopkins Univ. (April 1959).

3. Walker, R. E., Stone, A. R., and Shandor, M.: Secondary Gas Injection in a Conical Rocket Nozzle. AIAA J. 1,334-338 (1963).

4. Strike, W. T. and Schueler, C. J.: Investigation of Interference Effects Produced by Lateral Jets on Surfaces in a Supersonic Stream. AIAA Paper 63-184 (1963).

5. Sehgal, R. and Wu, J.: Thrust Vector Control by Liquid Injection into Rocket Nozzles. J. Spacecraft Rockets, 1,545-551 (1964).

6. Dowdy, M. W., and Newton, J. F., Jr.: Investigation of Liquid and Gaseous Secondary Injection Phenomena on a Flat Plate with M = 2.01 to M = 4.54. Jet Propulsion Lab., California Institute of Technology, Pasadena, Calif., TR 32-542 (December 1963).

7. Zukoski, E. E., and Spaid, F. W.: Secondary Injection of Gases into a Supersonic Flow. AIAA J., 2, 1689-1696 (1964).

8. Abramovich, G. N.: The Theory of Turbulent Jets (Massachusetts Institute of Technology Press, Cambridge, Mass.), English ed., Chap. 12, Sec. 4 (1963).

9. Vranos, A. and Nolan, J. J.: Supersonic Mixing of a Light Gas and Air. AIAA Propulsion Joint Specialists Conference, Colorado Springs, Colo. (June 1965); not preprinted.

10. Crist, S., Sherman, P. M., and Glass, D. R.: Study of the Highly Underexpanded Sonic Jet. AIAA J., 4, 68-71 (1966).

11. Adamson, T. C., Jr., and Nicholls, J. A.: On the Structure of Jets from Highly Underexpanded Nozzles into Still Air. J. Aero/Space Sci. 26, 16-24 (1959).

12. Schetz, J. A., and Billig, F. S.: Penetration of Gaseous Jets Injected into a Supersonic Stream. J. Spacecraft Rockets, 3, 1658-1665 (1966).

13. Orth, R. C., and Funk, J. A.: An Experimental and Comparative Study of Jet Penetration in Supersonic Flow. J. Spacecraft Rockets, 4, 1236-1242 (1967).

14. Schetz, J. A., and Billig, F. S.: Hydrogen Jet Penetration Studies (Analysis) (U) Aeronautics Division Quarterly Report (Confidential) Section VII/2b, APL/JHU AQR/66-1, (March 1966).

15. Orth, R. C., Billig, F. S., and Schetz, J. A.: Hydrogen Jet Penetration Studies (Analysis)(U). (Aeronautics Division Quarterly Report (Confidential) Section VII/4a APL/JHU AQR/66-2 (June 1966).

16. Orth, R. C., Funk, J. A., and Billig, F. S.: Hydrogen Jet Penetration Studies (Experimental)(U). Aeronautics Division Quarterly Report (Confidential)
    (a) Section VII/2c, APL/JHU AQR/66-1, (March 1966).
    (b) Section VII/4d, APL/JHU AQR/66-2, (June 1966).
    (c) Section III/26a, APL/JHU AQR/66-3, (September 1966).

17. Orth, R. C., and Schetz, J. A.: Gaseous Jet Penetration Studies (U). Aeronautics Division Quarterly Report (Confidential), Section III/19b, APL/JHU AQR/67-3, (September 1967).

18. Schetz, J. A.: Interaction Shock Shape for Transverse Injection (U). Aeronautics Division Quarterly Report (Confidential), Section III/24c, APL/JHU AQR/68-1, (March 1968).

19. Orth, R. C., Rice, J. L., and Billig, F. S.: Gaseous Jet Penetration Experiments (U). Aeronautics Division Quarterly Report (Confidential), Section III/21b, APL/JHU AQR/68-2, (June 1968).

20. Hoerner, S.: Fluid Dynamic Drag (published by author, 1958).

21. Schetz, J. A., Hawkins, P. F., and Lehman, H.: The Structure of Highly Underexpanded, Transverse Jets in a Supersonic Stream. AIAA J. 5, 882-884 (1967).

22. Lucero, E. F.: Turbulent Boundary Layer Separation Induced by Three Dimensional Protuberances on a Flat Plate. M. S. Thesis, Department of Aerospace Engineering, Univ. of Maryland (1966).

23. Johns, T.: Gas Chromatography Application Manual. Beckman Instruments, Inc., Fullerton, Calif. (1959).

24. Pai, S.: Viscous Flow Theory II-Turbulent Flow. (D. VanNostrand Company, Inc., Princeton, N.J.), Chap. VI, p. 102, (1957).

25. Eckert, E. R. G., and Drake, R. M., Jr.: Heat and Mass Transfer. (McGraw-Hill Book Company, Inc., New York, 1959), 2nd ed., Chap. VI. p. 144.

26. Broadwell, J. E.: Analysis of the Fluid Mechanics of Secondary Injection for Thrust Vector Control. AIAA J., 1, pp. 1067-1075 (1963).

27. Karamcheti, K., and Hsia, H. T-S.: Integral Approach to an Approximate Analysis of Thrust Vector Control by Secondary Injection. AIAA J., 1, pp. 2538-2544 (1963).

28. Hsia, H. T-S., Seifert, H., and Karamcheti, K.: Shock Induced by Secondary Fluid Injection. J. Spacecraft and Rockets, 2, pp. 67-72 (1965).

29. Billig, F. S.: Shock-wave Shapes Around Spherical and Cylindrical-nosed Bodies. J. Spacecraft and Rockets, 4, pp. 822-823 (1967).

30. Schetz, J. A., Weinraub, R., and Mahaffey, R.: Supersonic Transverse Injection in Supersonic Flow. AIAA J., 6, (1968).

31. Chapman, D. R., Kuehn, D. M., and Larson, H. K.: Investigation of Separated Flows in Supersonic and Subsonic Streams with Emphasis on the Effect of Transition. NACA Rept. 1356 (1958).

NASA-Langley, 1969 —— 12 CR-1386